

THESIS FOR THE DEGREE OF DOCTOR OF PHILOSOPHY

SOLIDS MIXING IN BUBBLING FLUIDIZED BEDS

Erik Sette

Department of Energy and Environment

CHALMERS UNIVERSITY OF TECHNOLOGY

Göteborg, Sweden 2016

Solids mixing in bubbling fluidized beds
Erik Sette
ISBN 978-91-7597-347-0

© Erik Sette 2016

Doktorsavhandling vid Chalmers tekniska högskola
Ny serie Nr. 4028
ISSN 0346-718X

Department of Energy and Environment
Division of Energy Technology
Chalmers University of Technology
SE-412 96 Gothenburg
Sweden
Telephone +46 (0)31-772 1000

Chalmers Reproservice
Göteborg 2016

Cover: The cover image shows a cut through a fluidized bed with a bulk solids cross-flow. The bed surface shows the velocity field induced by the cross-flow and the cut shows the bubble induced flow structures.

Solids mixing in bubbling fluidized beds

Erik Sette

Department of Energy Technology

Chalmers University of Technology

SE-412 96 Gothenburg (Sweden)

Abstract

For solid fuels, thermochemical conversion processes such as combustion and gasification are especially suitable to be carried out in fluidized bed units because of the relatively high mixing rates, fuel flexibility and the possibility to use active bed material to enhance process efficiency. Mixing of fuel is important to ensure complete conversion and reduced emissions of unburnt material. Furthermore, mixing of the bulk material has its importance in that it governs the variations of the temperature field across the bed. Thus, in order to optimize the operation of existing units and the design of new units, there is a need to understand and quantify solids mixing.

Despite solids mixing in fluidized beds having been investigated for several decades, there is still lack of knowledge in the area. A common approach is to quantify mixing using a dispersion coefficient. However, values for the dispersion coefficients published in literature are scattered over several orders of magnitude and have often been derived from small units operated at ambient conditions, *i.e.* are not representative for industrial scale fluidized beds.

In the present work methods are presented to evaluate lateral mixing for both the bulk solids and fuel particles and vertical mixing of fuel. The experimental work is conducted in fluid-dynamically downscaled units and a large-scale unit, *i.e.* the results are relevant for commercial conditions. A novel 3-dimensional particle tracking system based on anisotropic magneto resistance sensors has been implemented which provides detailed information about flow structures of the solids found within the bed. Furthermore a novel camera probe has been used to enable tracking of several fuel particles in an industrial scale bed operated at elevated temperature.

The lateral dispersion coefficients for bulk solids obtained in the present work are two orders of magnitude larger than what has been published in literature previously, which is explained by the application of fluid dynamic scaling to study large-scale units. Since wall effects are of

less importance in large scale equipment the data provided in the present work is of more relevance to industrial units than previous data found in literature. Values of the lateral dispersion coefficients obtained for fuel particles in fluid-dynamically downscaled units in this work are of the same order of magnitude as data obtained in industrial scaled equipment operating at elevated temperatures. This shows that application of fluid-dynamic downscaling can be applied to predict fuel mixing in large scale fluidized beds.

Lateral solids dispersion is generally found to increase with fluidization velocity and bed height, with an enhanced effect for beds with a gas distributor providing a high pressure drop. The presence of a continuous flow of bulk solids across the fluidized bed is found to create a convective contribution to solids mixing which fuel particles are found to follow to different extents. Mathematical models are applied to account for such convective flow of bulk and fuel particles. Furthermore this continuous flow of bulk solids is found to decrease the vertical segregation of fuel particles in an industrial scale fluidized bed.

Keywords: Solids mixing, lateral dispersion, fluid-dynamic scaling, solids cross-flow

List of publications included in the thesis

- I. Erik Sette, David Pallarès, Filip Johnsson. Experimental evaluation of lateral mixing of bulk solids in a fluid-dynamically down-scaled bubbling fluidized bed. *Powder Technology* 263, pp. 74-80, 2014
- II. Erik Sette David Pallarès, Filip Johnsson, Experimental quantification of lateral mixing of fuels in fluid-dynamically down-scaled bubbling fluidized beds. *Applied Energy* 136, pp. 671-681, 2014.
- III. Erik Sette, David Pallarès, Filip Johnsson, Fredrik Ahrentorp, Anders Ericsson, Christer Johansson. Magnetic tracer-particle tracking in a fluid dynamically down-scaled bubbling fluidized bed. *Fuel Processing Technology* 138, pp. 368-377, 2015.
- IV. Erik Sette, Anna Köhler, David Pallarès, Filip Johnsson, Real-time 3-dimensional tracking of a fuel particle in a fluid-dynamically down-scaled fluidized bed. *To be submitted*.
- V. Erik Sette, David Pallarès, Filip Johnsson, Influence of bulk solids cross-flow on fuel residence time in fluidized beds. *Fuel Processing Technology* 140, pp. 245-251, 2015.
- VI. Erik Sette, Teresa Berdugo Vilches, David Pallarès, Filip Johnsson. Investigation of fuel mixing under industrial fluidized-bed conditions using a digital video camera. *Applied Energy* 163, pp. 304-312, 2016.

Erik Sette is the principal author of Papers I–VI. Associate Professor David Pallarès is the assistant academic supervisor and has contributed with discussion and editing of all six papers. Professor Filip Johnsson is the principal academic supervisor and has contributed with discussion and editing of all six papers. Fredrik Ahrentorp, Anders Ericsson, and Christer Johansson have developed the magnetic particle tracking method and co-authored Paper III. Anna Köhler has carried out the experimental work in Paper IV and contributed with editing of Paper IV. Teresa Berdugo Vilches contributed to the experiments carried out in Paper VI and helped with the editing of the paper; she is the person responsible for the evaluation of the vertical mixing.

Additional work has been carried out during the course of the work, resulting in the papers listed below. These have not been included in the thesis since the contents either overlap with those of papers already included in the thesis or are considered to be outside the scope of the thesis.

List of publications not included in the thesis

- I. Erik Sette, Alberto Gómez García, David Pallarès, Filip Johnsson. Quantitative evaluation of inert solids mixing in a bubbling fluidized bed. Proceedings of the 21st International Conference on Fluidized Bed Combustion, pp.573-580, Naples, Italy, 2012.
- II. Erik Sette, Sonia Aimé, David Pallarès, Filip Johnsson. Analysis of lateral fuel mixing in a fluid-dynamically down-scaled bubbling fluidized bed. Proceedings of the Fluidization XIV conference, pp. 877-884, Noordwijkerhout, The Netherlands, 2013.
- III. Erik Sette, David Pallarès, Filip Johnsson. The influence of operating conditions and fuel-feeding location in fuel residence time in an indirect gasifier. Proceedings of the 11th International Conference on Circulating Fluidized Beds, Beijing, China, 2014.
- IV. Jens Olsson, Joakim Larsson, Erik Sette, David Pallarès, Filip Johnsson. Experimental evaluation of the lateral mixing of fuel in a fluidized bed with cross-flow of solids – influence of tube banks. Proceedings of the 11th International Conference on Circulating Fluidized Beds, Beijing, China, 2014.
- V. Teresa Berdugo Vilches, Erik Sette, Henrik Thunman. Behavior of biomass particles in a large scale (2-4 MW_{th}) bubbling bed reactor. WIT Transactions on Engineering Science-Computational Methods in Multiphase Flow VIII, vol. 89, pp. 151-160. 2015.
- VI. Erik Sette, David Pallarès, Filip Johnsson. Camera-probe fuel tracking under industrial fluidized-bed conditions. Proceedings of the 22nd International Conference on Fluidized Bed Conversion, Turku, Finland, 2015.
- VII. David Pallarès, Erik Sette, Filip Johnsson, Fredrik Ahrentorp, Anders Ericsson, Christer Johansson, Jakob Blomgren, Christian Jonasson. 3-dimensional magnetic particle tracking in a fluid-dynamically downscaled bubbling fluidized bed. Proceedings of the 22nd International Conference on Fluidized Bed Conversion, Turku, Finland, 2015.
- VIII. Erik Sette, Anna Köhler, David Pallarès, Filip Johnsson. 3-dimensional particle tracking in a fluid-dynamically downscaled fluidized bed using magneto resistive sensors. The 8th International Symposium on Coal Combustion, Beijing, China, 2015.
- IX. Anton Larsson, Erik Sette, David Pallarès, Claes Breitholtz, Henrik Thunman. Char conversion in the Chalmers 2–4-MW_{th} dual fluidized bed gasifier. *To be submitted.*
- X. Antonio Soria, Erik Sette, David Pallarès, Filip Johnsson. Modeling the motion of low-density char particles on the surface of a bubbling fluidized bed. *To be submitted.*
- XI. Henrik Ström, Erik Sette, David Pallarès, Numerical and experimental investigation of temperature effects on fluidization behavior. *To be submitted.*

Acknowledgments

I am very grateful to my supervisor Associate Professor David Pallarès who has given me much help and support throughout the work. I especially appreciate David's skills in visualizing complex concepts in simple drawings. I would like to thank my examiner Professor Filip Johnsson at Chalmers University of Technology for the opportunity to work at the Department of Energy and Environment, Division of Energy Technology. I would like to thank for the financial support given by: Swedish gasification centre (SFC), Akademiska Hus, Valmet AB, Göteborg Energi, the Swedish energy agency, E.ON and Chalmers Energy Area of Advance.

I appreciate all material provided online by Professor Stephen Boyd on Linear Dynamical Systems and Convex Optimization, my work would not have been as fruitful without it. Furthermore, I have received much help from numerous project assistants and master thesis workers and I would like to thank them all. An extra warm "thank you" is given to the research assistants, Ulf, Rustan, Johannes and Jessica for all their help in the experimental work and to the administrative staff at the division, Inger, Katarina and Marie.

I would like to thank the Gasification group for all interesting discussions and fun moments. A special thanks goes to Alberto Alamia for making the hours in the office much more enjoyable. Furthermore, I would like to give special thanks to: "My dear deer" Jelena, "Mi arma" Teresa and the "Islandic heroine" Stefania for our friendship. I would also like to thank my more recent friends Tove and Angelica.

To all colleges at the division of energy technology thank you for being you!

I would like to thank my family for all encouragement and support and awakened my interest for science and technology almost 30 years ago.

The greatest thanks goes finally to Kerstin for your patience with me, you are my everything and I love you truly!

Erik Sette

Göteborg, 2016

Contents

List of publications included in the thesis	iii
List of publications not included in the thesis	iv
Acknowledgments	v
1 Introduction	1
1.1 Aim	2
2 Background	4
2.1 Previous experimental work on solids mixing	4
2.2 Solids mixing theory	5
2.2.1 Modeling the dispersive mixing	8
2.2.2 Models that account for solids cross-flow	10
3 Fluid-dynamic downscaling	12
4 Experimental setup	15
5 Overview of available experimental methods for studying solids mixing	19
5.1 Tomographic methods	19
5.2 Particle tracking methods	20
6 Data evaluation	23
6.1 Indirect methods	23
6.2 Direct methods	24
6.3 Kalman filtering	25
6.4 Principal component analysis	26
7 Results	27
7.1 Existence of mixing cells	27
7.2 Lateral dispersion without cross-flow	29
7.3 Solids mixing with cross-flow	32
7.4 Pyrolysis time of fuel particles	35
7.4.1 Additional information obtained with the hot camera probe	37
8 Conclusions	39
8.1 Bed material	39
8.2 Fuel	39
9 Future work	41
9.1 Particle tracking in 3 dimensions	41
9.2 Additional possibilities with camera measurements	41
9.3 Further investigations of cross-flow	41

1 Introduction

Thermal conversion processes of solid fuels, such as combustion and gasification, are suitable to be carried out in fluidized beds due to the relatively high mixing rates and fuel flexibility of these units. Fluidized beds can be classified as either bubbling or circulating depending on the velocity of the gas that is fed into the bed in relation to the terminal velocity of the particles; a circulating bed requires auxiliary equipment to separate and recirculate the bed solids. Bubbling fluidized beds are used in small- and medium-scale boilers for combined heat and power (CHP) applications [1] and in large gasifiers [2-5], whereas circulating fluidized beds are employed in both medium-sized CHP and large power boilers (up to several hundreds of MW_{el}) [1]. In the fluidized beds used for solid-fuel conversion, the solids can be divided into at least two types: bed material (also called bulk solids); and fuel particles. Other solids may be added as needed, *e.g.*, limestone for sulfur capture when burning high-sulfur coal. Fuel particles, which are typically coarser, lighter, and have more irregular shapes than the inert bed material (make-up material or bed ash), usually constitute a mass fraction of <5%.

Fluidized beds are capable of handling several fuel types, and in recent years, in large part due to the need to reduce anthropogenic CO₂ emissions, research has focused on the use of biomass and waste products. Compared to fossil fuels such as coal, these fuels are characterized by high contents of moisture and volatile compounds, which are characterized by their fast release rates. Thus, the lateral mixing of the fuel is a key parameter that needs to be controlled, so as to improve the performance profiles of fluidized bed boilers and gasifiers.

In boilers, sufficiently fast lateral mixing is required to minimize the number of fuel feeding ports and to ensure even fuel distribution over the entire bed cross-section [6]. Too slow lateral mixing of the fuel may result in maldistribution of the volatiles, with the consequence of emissions of unburnt volatile matter and the promotion of hot-spots within the boiler [7]. To counteract this, one must apply higher air-to-fuel ratios, which reduce boiler performance and increase the operational and capital costs related to fan power and flue gas cleaning.

For fluidized bed indirect gasifiers (so-called 'allothermal gasifiers'), which are connected to a combustor that generates the heat needed for the endothermic gasification reactions [2, 3], lateral mixing of fuel has to be maintained at a moderate level to allow the fuel sufficient time to become gasified (which is a slower conversion process than combustion [8]). Thus, an increase in lateral mixing results in an increased loss of char from the gasifier to the connected boiler, where it is combusted [2].

Regarding mixing in the vertical direction, fluidized bed boilers and gasifiers at the commercial scale have large cross-sectional bed areas and are operated with a low bed aspect ratio (height-to-width ratio of the dense bed) [9], which makes solids mixing in the axial direction less critical than mixing in the lateral direction in the dense bed [10]. The fuel and bed material

are affected to different extents by the action of the rising bubbles owing to differences in their physical properties (*i.e.*, size, shape, and density). It was first described by Rowe et al. [11] that lighter particles (flotsam) are preferentially dragged upwards by the bubbles, while the denser material (jetsam) tends to sink to the bottom of the bed. In the case of fuel particles, the difference in density between the bed material and the fuel may lead to segregation, *i.e.*, a lack of vertical mixing [12, 13]. The rapid release of volatiles from the fuel may induce so-called ‘endogenous bubbles’ and amplify the floating behavior of the fuel particles [14, 15].

While several studies of solids mixing in fluidized beds have been conducted, data relevant to industrial-scale beds operated at elevated temperatures are scarce. Furthermore, in dual fluidized bed (DFB) systems, an additional mixing phenomenon induced by the solids cross-flow is introduced, which has not previously been investigated. In the present work, experimental data for industrial-scale fluidized beds are presented and simplified models for describing the solids mixing are presented and validated.

1.1 Aim

The aim of this work is to achieve a quantitative understanding of the mixing of solids, *i.e.*, the bed material and fuel particles, in the dense bottom region of fluidized beds, in order to improve the rate of conversion of fuel in combustion and gasification applications. The work is mainly experimental, with measurements conducted in three fluid-dynamically downscaled cold flow models and in an industrial-scale indirect gasifier operated at high temperature. In addition, mathematical models for the lateral mixing of fuel are formulated and validated using the obtained experimental data.

The six papers of this thesis describe studies in which different measurement methods has been applied, as schematized in Figure 1. The investigations in Papers I–V are conducted at cold flow conditions using fluid-dynamic downscaling, while Paper VI uses measurements of the fuel mixing at high temperature. A summary of the topic covered in each paper is given below:

Paper I presents an investigation of the lateral mixing of bulk solids in bubbling fluidized beds without any solids cross-flow, *i.e.*, stationary beds. The effects of different operational parameters and the gas distributor are studied.

Paper II evaluates the relationship between the lateral mixing of the bed material and the different fuel types. A cold flow model of a stationary bubbling fluidized bed is used in which the fuel particles are tracked using a video camera that records the motion of the fuel particle on the surface of the bed.

Paper III introduces a novel particle tracking method that is based on magnetism, which allows for 3-dimensional particle tracking in a fluid-dynamically downscaled bed. This method provides information about particle trajectory and rotation with high spatial and temporal resolutions.

Paper IV applies the method developed in Paper III to obtain a deeper understanding of flow structures in a 3-dimensional bed. The presence of mixing cells in a 3-dimensional bed is shown, and the influence of the gas distributor characteristics on the particle concentration within the bed is investigated.

Paper V investigates the mixing of fuel particles in a DFB system by sampling the residence time distributions of batches of fluid-dynamically downscaled fuel particles. In systems of interconnected beds, there exists a continuous flow of bulk solids between the reactors, which represents an additional mixing mechanism. This paper explores the possibility of applying simplified mathematical models to describe this mechanism.

Paper VI uses a video camera to investigate the lateral mixing and vertical segregation of the fuel particles in an industrial-scale fluidized bed that is operated at high temperature. The influence of cross-flow (discussed in Paper V) is also investigated.

	<i>Cold conditions:</i>	<i>Hot conditions:</i>
B u l k	Paper I: Tracer sampling	
F u e l	Paper II: Optical (without cross-flow) Paper III: 3D tracking (development) Paper IV: 3D tracking (applied) Paper V: Tracer sampling (with cross-flow)	Paper VI: Optical (with cross-flow)

Figure 1: The order and contents of the papers included in the thesis.

2 Background

Solids mixing in fluidized beds has been investigated for several decades (see the review of Breault [16]). In spite of this, there remains a lack of knowledge in this area, mainly because of the difficulties associated with performing measurements in large-scale fluidized beds and the fact that numerical simulations are too computationally expensive to provide a detailed understanding of the mixing phenomena. Here follows a summary of the literature, which includes both experimental investigations and theoretical studies.

2.1 Previous experimental work on solids mixing

The experimental work conducted on solids mixing has looked at either the bulk bed material [17-30] or larger and lighter particles, which can be taken as representative of fuel particles [31-50]. Furthermore, the experimental apparatuses used in previous studies have varied in terms of size (mostly at the laboratory scale but some works at a larger scale [37, 51]), geometry (narrow tubes, wider pseudo-2-dimensional units or 3-dimensional beds), and operational conditions (cold or hot). An alternative to conducting experiments in industrial-sized units is to apply fluid-dynamic downscaling (see Section 3). Fluid-dynamic downscaling is a validated [45, 52-54] and convenient way for obtaining under cold flow conditions results that are quantitatively representative of large-scale beds operated under hot conditions.

Figure 2 outlines the influences of bed geometry and fluid-dynamic scaling on the lateral mixing of bed materials. The values for the lateral dispersion coefficients obtained in pseudo-2-dimensional beds are typically lower than the values obtained in 3-dimensional beds (both cold flow and downscaled), most likely as a consequence to the confined flow expected in pseudo-2-dimensional beds. When fluid-dynamic downscaling is applied, the coefficients for lateral dispersion are found to be larger than those for non-fluid-dynamically scaled 3-dimensional cold flow beds under comparable operational conditions. Thus, while studies conducted using pseudo-2-dimensional units and non-scaled 3-dimensional units can yield useful qualitative knowledge about solids mixing, there is a need for quantitatively valuable knowledge, which can be acquired by measuring in either large-scale beds or fluid-dynamically scaled units (to the authors' knowledge, there are no available data regarding bed material dispersion in industrial-sized equipment at high temperature).

In Paper II, it is proven for the first time that fluid-dynamic downscaling applies to the mixing of fuel particles, which supplements the previously verified scaling of the mixing of bed material. A comparison of the lateral dispersion coefficients for solids, including fuel particles, is described in Section 7.

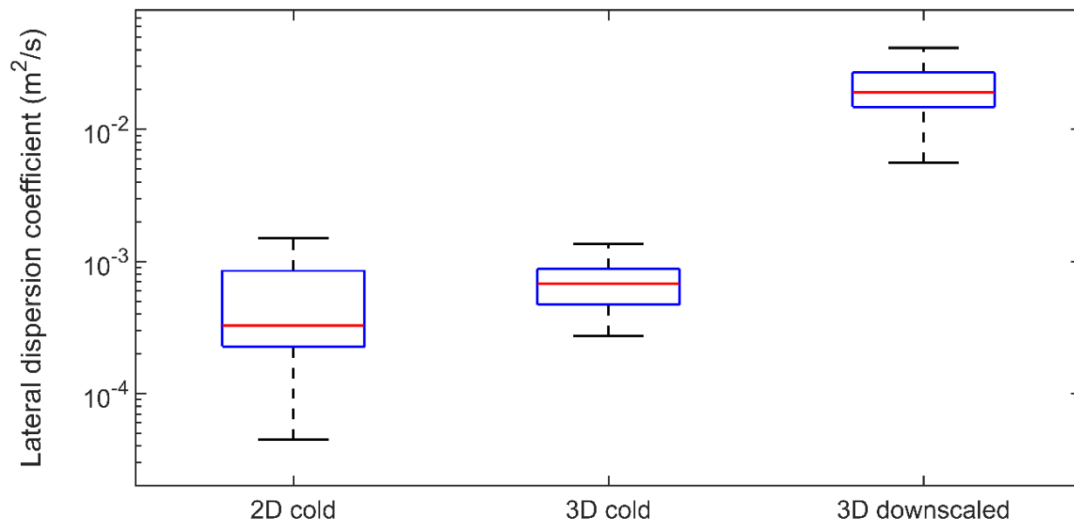


Figure 2: Lateral dispersion coefficients for bed material obtained for various arrangements of the experimental apparatus. Data taken from [18, 24, 26-28, 30].

Evaluation of the mixing of the bed material in the bottom region of an industrial unit is challenging. Bed material mixing is evaluated by either sampling batches of a tracer substance or tracking a single bed material particle. Batch sampling involves the collection of samples from a hot bed, which is difficult and time-consuming and cannot be easily executed with sufficient time resolution to resolve the features of the solids flow. Single-particle tracking using X-rays or radioactive tracer particles is in theory possible, although it requires large pieces of equipment that are hard to fit into boilers, making single-particle tracking unfeasible. Finally, magnetic particle tracking is not suitable for industrial applications, since the magnetic field of permanent magnet tracers decays with increasing temperature.

2.2 Solids mixing theory

It is generally accepted that the gas bubbles that rise through the bed are responsible for solids mixing. Three main mechanisms of solids mixing that relate to the bubble flow have been proposed in literature [55], namely:

- 1) Lifting in the wake of a rising bubble.
- 2) Sinking in the emulsion around the rising bubble, to fill the gap created by bubbles.
- 3) Splashing at the surface of the bed when a bubble erupts.

The three mechanisms are presented graphically in Figure 3. The figure also shows that bubbles increase in size, as a result of bubble coalescence, as they rise along the bed. Just before a bubble erupts at the surface, the height of the bed is increased locally and at the time of eruption, the bed height is reduced locally to below the time-averaged level.

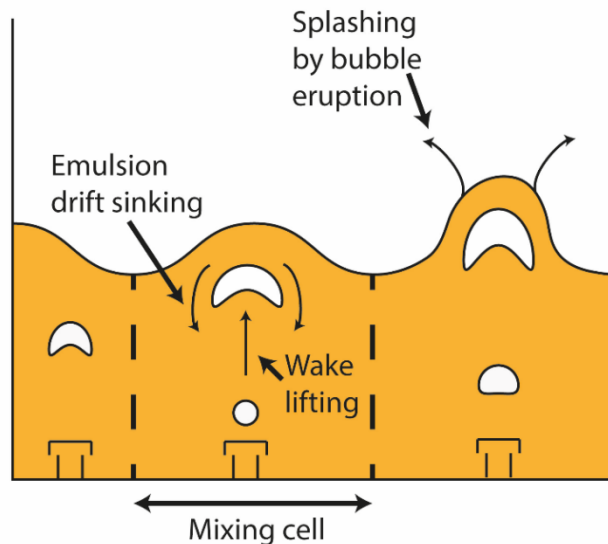


Figure 3: Main mechanisms of solids mixing in relation to the bubble flow, as proposed in the literature. Rising gas bubbles are responsible for all three mechanisms.

It has been experimentally determined that gas bubbles rise in preferential pathways, called bubble paths [56]. Around each of these bubble paths a toroidal solids flow pattern (yielding two vortices in a vertical 2-dimensional cut) have been detected by analyzing the trajectory of a tracer particle that mimics a fuel particle [40]. The region that encompasses the bubble path and the surrounding local flow structure has been denoted as ‘a mixing cell’ by Pallarès et al [40], whose experiments showed that fuel particles tend to populate the borders of a mixing cell rather than the bubbles paths. Figure 3 shows a mixing cell and the main solids mixing mechanisms responsible for the exchange of material between the mixing cells.

The growth of a bubble can be reduced by the insertion of a tube bank, as shown by Andersson et al. [57]. The gas bubbles can, provided they have sufficiently high velocity, break down, thereby resulting in what Andersson et al. [57] refer to as a ‘multiple bubble regime’, which creates a more even distribution of gas bubbles; as a consequence, solids mixing is improved.

Regarding diagnostics, a common method to characterize fluidization is to measure pressure fluctuations. Baskakov et al. [58] linked the features in such measurements to bubble-related phenomena inside the bed. Figure 4a shows an example of a time series of pressure measurements. The pressure signal can be explained in the following way for a simplified case with a narrow bed in the single bubble regime [59]. As a bubble approaches the surface and until just before its eruption, the bed height is locally increased above the time-averaged height, as shown schematically in Figure 3. This event increases the pressure signal above the average value. As the bubble erupts at the bed surface, a sharp and rapid decrease occurs in the pressure signal, since the bed height is locally reduced where the bubble emerged, yielding the characteristic low pressure drops associated with bubble eruption.

It is common practice to analyze the pressure signal in the frequency domain rather than the time domain, by computing the power spectrum density of the signal [60]. The power spectrum density of the pressure signal shown in Figure 4a is plotted in Figure 4b. A clear peak is evident in the spectrum and is referred to as the characteristic bubble frequency, *i.e.*, corresponding to a bubble cycle, provided that the bed is in the single or exploding bubble regime [59], with typical values in the range of 1–5 Hz. In addition, if the cross-section is much greater than the bed height, there will be room for a number of bubble paths over the cross-section. This means that a pressure measurement in the reactor wall will yield an average for all the bubble passages, resulting in a broader power spectrum. The amplitude of the peak is associated with the bubble size: the larger the bubbles, the larger the pressure fluctuations, *i.e.*, the larger the amplitude.

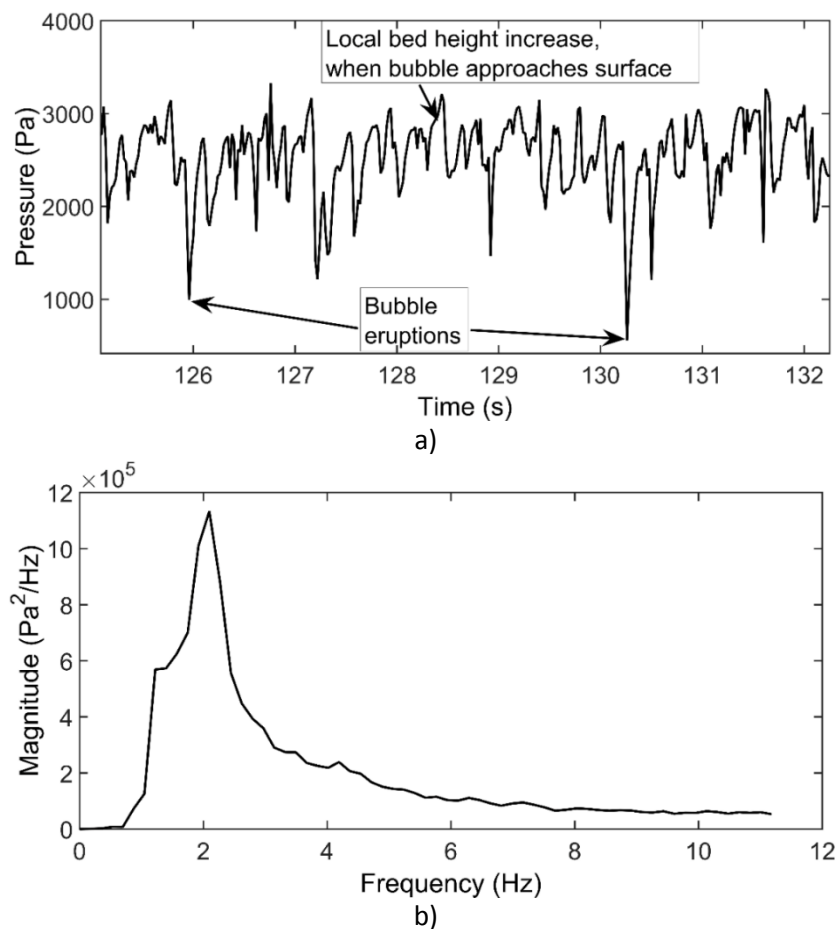


Figure 4: a) Differential pressure between the atmosphere and the dense bed (measured 0.03 m above the gas distributor). Just before a bubble erupts, the height of the bed is increased locally, which results in a small increase in pressure, which is followed by bubble eruption. Bubble eruptions yield a rapid decrease in pressure. b) Power spectrum density of the pressure signal in Figure 4a. The peak occurs at the characteristic frequency of the bed. Taken from Paper I.

2.2.1 Modeling the dispersive mixing

In large-scale fluidized beds, several mixing cells co-exist across the cross-section, each of which is related to a single bubble path. Since bubbles coalesce as they rise, the number of mixing cells is not necessarily equal to the number of nozzles in the gas distributor, although it does depend on the height of the dense bed. To describe mathematically on the macroscopic level the transient solids concentration in a fluidized bed, the solids that are located within any mixing cell are assumed to have equal probability of moving to any of the neighboring mixing cells. This is an example of a Markov chain, which is mathematically described by the diffusion equation:

$$\frac{\partial C_f}{\partial t} = D \nabla^2 C_f \quad (1)$$

However, as Eq. (1) is applied to describe the solids flow macroscopically, the coefficient D in the equation is termed the dispersion coefficient rather than the diffusion coefficient, since the mixing results from a highly convective bubble flow. The dispersion coefficient is usually determined experimentally.

For 3-dimensional beds, the exchange of material between mixing cells is in this work assumed to occur only between orthogonally neighboring mixing cells, as shown in Figure 5. Obviously, during the experiments, the material will also be scattered to the diagonal cells. This is taken into account in the model by allowing half of the scattered material to exchange between two perpendicular cells.

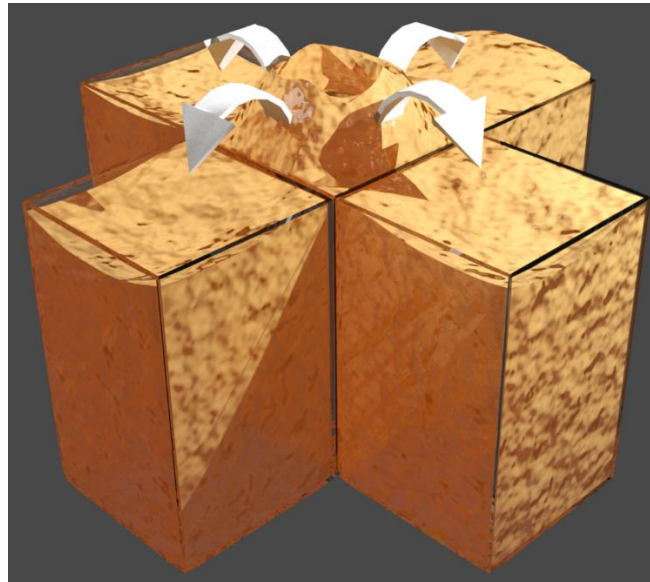


Figure 5: Mixing cells in a 3-dimensional bed extend along the two lateral directions. Scattering to diagonal cells is accounted for in the model by allowing half of the scattered material to exchange between two perpendicular cells.

The validity of Eq. (1) for describing the lateral mixing of fuel on a macroscopic level is shown in Figure 6, which compares the fuel concentration found experimentally by Olsson et al. [39] (solid line) to the solution derived from Eq. (1) (dashed line). It is clear that the solution to Eq. (1) estimates well the measured concentration on a macroscopic scale, *i.e.*, the model can describe the exchange of material between mixing cells. However, the diffusion model is unable to capture the local/mesoscopic minimums and maximums related to the bubble paths and their surrounding solids-rich regions. In Paper VI, the observations made under cold conditions by Olsson et al. [39] are confirmed also under hot conditions, and it is found that the solids cross-flow influences the mixing cells by smoothing them out.

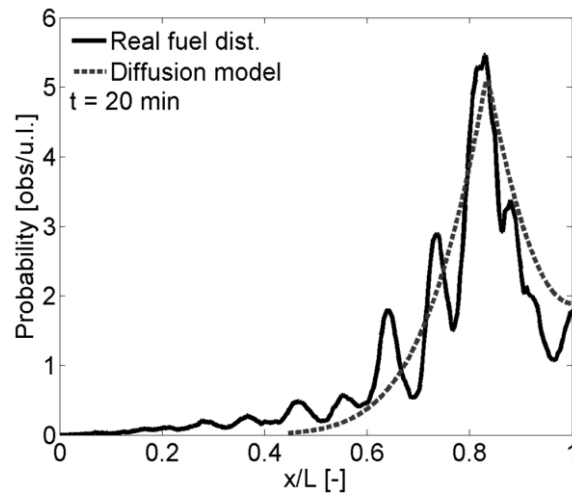


Figure 6: Spatial distribution of the probability of observing a fuel particle was experimentally determined by Olsson et al. [39]. The local minimum points correspond to the location of a bubble path.

An initial step towards investigating lateral solids mixing in greater detail than allowed by the experimentally determined values of the dispersion coefficients, D , was taken by Olsson et al. [39]. They combined these values with the parameters of bed frequency, f , and cell mixing size, L , in order to extract information regarding solids exchange between mixing cells. In the present work, this approach is applied and the so-called ‘bubble mixing factor’, β , which ascertains which share of the solids in a mixing cell is exchanged at each bubble cycle, is determined from experimental data using Eq. (2). The characteristic frequency is typically determined from pressure fluctuation measurements, such as those shown in Figure 4. The characteristic length of the mixing cells, L_{cell} , is in the present work estimated visually by inspecting the location at which the bubbles erupt, which entails a relatively high level of uncertainty.

$$\beta = \frac{2 \cdot D}{f \cdot L_{cell}^2} \quad (2)$$

The bubble mixing factors and lateral dispersion coefficients are determined under different operational conditions and analyzed for bed material and fuel particles (three different types) in Papers I and II, respectively.

2.2.2 Models that account for solids cross-flow

In the case of a system with interconnected fluidized beds, such as an indirect gasification unit [61, 62] or chemical looping combustion unit [63, 64], a continuous flow of the circulating bulk solids crosses each reactor. This cross-flow of bulk solids creates in the dense bed a convective flow field, which affects solids mixing and has to be considered to come up with an accurate description of the solids mixing (see Figure 7).

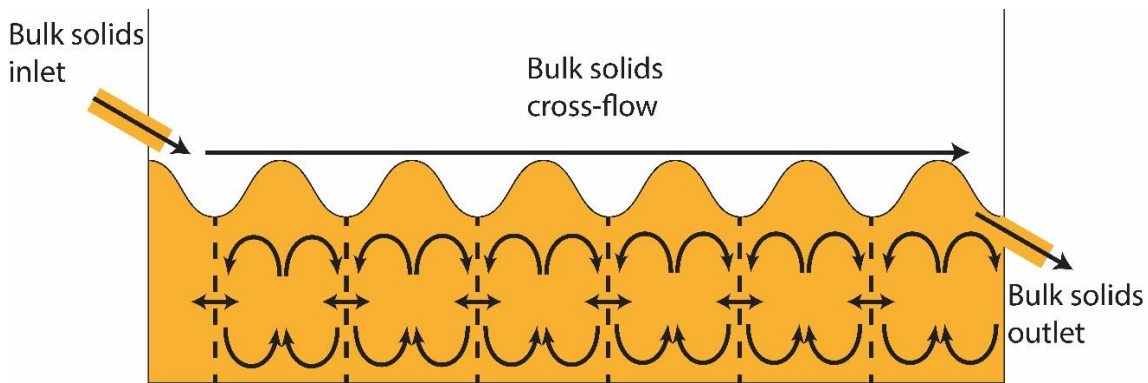


Figure 7: A convective flow field is superimposed on the dispersive flow as an effect of the flow of bulk solids through the dense bed. Taken from Paper V.

The horizontal velocity field of the bed material in a dense bed, \mathbf{u} , is difficult to measure; in Paper V, it is modeled using the potential flow theory, *i.e.* determining a vector field (in this case a velocity field) from the gradient of a scalar field [65]. Assuming that the transport of bed material occurs through dispersive lateral mixing (Kunii and Levenspiel [66]), a diffusion equation can describe the lateral transport, *i.e.*, Eq. (1). By solving Eq. (1) and evaluating the gradient of the solution, a vector field is derived. Details of the modeling approach and the validation thereof are presented in Paper V. A second method for modeling the velocity field is outlined in the *Results* section (Section 7.3) of the present work.

Since the mixing of fuel particles is affected by the solids cross-flow, the transport equation that describes the fuel concentration needs to be modified to include a convective term. This yields Eq. (3), where \mathbf{u} is the velocity field created by the solids cross-flow and θ is a cross-flow impact factor that accounts for how well the fuel follows the convective flow of the bed material.

$$\frac{\partial C_f}{\partial t} + \nabla \cdot (C_f \theta \mathbf{u}) = \nabla \cdot (D_f \nabla C_f) \quad (3)$$

When experimentally determining lateral solids dispersion coefficients, if neither measurements nor reliable modeling of the velocity field are available, the convective contribution of the solids cross-flow can be lumped into the dispersive mixing of the bed material, yielding a modified version of Eq. (1):

$$\frac{\partial C_f}{\partial t} = \frac{\partial}{\partial x} \left((D_x^{bubble} + D_x^{cross}) \frac{\partial C_f}{\partial x} \right) + \frac{\partial}{\partial y} \left((D_y^{bubble} + D_y^{cross}) \frac{\partial C_f}{\partial y} \right) \quad (4)$$

Note that if the velocity field is different in the two lateral directions the apparent dispersion will appear as non-isotropic, *i.e.*, the lumped dispersion coefficients in the two lateral directions will no longer be equal, as concluded from Eq. (4). The experiments described in Paper VI were conducted in an industrial-scale fluidized bed with a significant level of cross-flow. Since no measurements are available regarding the convective flow of the bed material, Eq. (4) can be applied to evaluate the lumped lateral mixing of the fuel particles.

3 Fluid-dynamic downscaling

The experimental work described in Papers I–V was performed in three fluid-dynamically down-scaled cold flow models. By employing fluid-dynamic scaling, two fluidized beds of different scales and with different temperature levels could be operated so as to generate similar fluid dynamics. Proper scaling of a reactor implies fulfilling two similarities: 1) geometric *i.e.*, the ratio between corresponding lengths is constant in the two systems; and 2) dynamic, *i.e.*, forces acting on the system have a constant ratio at all locations [67]. There are two different approaches to achieving similarity between reactors: Buckingham’s π -theorem [68]; and non-dimensionalizing the governing equations and boundary conditions. However, both approaches yield the same results. Glicksman et al. [52] applied the second approach to fluidized beds by deriving the governing equations for the motion of a multiphase continuum and for individual solid particles in a dimensionless form. Thus, Glicksman's scaling laws are based on the partial differential equations for continuity of the gas and solid phases, Eqs. (5) and (6), and for momentum transport of the same phases, Eqs. (7) and (8).

$$\frac{\partial \epsilon}{\partial t} + \nabla \cdot (\epsilon \mathbf{u}) = 0 \quad (5)$$

$$\frac{\partial}{\partial t} (1 - \epsilon) + \nabla \cdot [(1 - \epsilon) \mathbf{v}] = 0 \quad (6)$$

$$\rho_f \epsilon \left[\frac{\partial \mathbf{u}}{\partial t} + \mathbf{u} \cdot \nabla \mathbf{u} \right] + \rho_f g \epsilon - \nabla \cdot \mathbf{E}_f + \mathbf{F} = 0 \quad (7)$$

$$\rho_s (1 - \epsilon) \left[\frac{\partial \mathbf{v}}{\partial t} + \mathbf{v} \cdot \nabla \mathbf{v} \right] + \rho_s g (1 - \epsilon) - \nabla \cdot \mathbf{E}_p - \mathbf{F} = 0 \quad (8)$$

Based on Eqs. (5) to (8), Glicksman et al. [52] derived a number of dimensionless parameters (see Table 1), which need to be kept constant to achieve similarity of the results obtained in the two systems. If all these relationships are kept constant, the scaling is referred to as applying the full set of scaling laws. However, the full set of scaling laws places constraints as to which scaling factor can be used. Therefore, Glicksman et al. [69] developed a simplified set of scaling laws that allows for more flexibility in choosing the scaling factor. The simplified set of scaling laws is valid in two different flow regimes: 1) the viscous-dominated region, which is typical for beds with small particles and low fluidization velocities, where inertial effects are negligible; and 2) the inertial-dominated regime, which is typical for beds with large particles and high gas velocities, where viscous effects are negligible. A different set of scaling laws for bubbling fluidized beds was developed by Horio et al. [70], and this was subsequently shown by Glicksman et al. [69] to be equivalent to Glicksman’s simplified scaling laws for the viscous regime. In the present work, Glicksman’s full set of scaling laws is applied, which means that

the parameters in Table 1 are kept constant in the different fluidized beds used. The length scaling factor is obtained as follows:

$$L = \left[\frac{\left(\frac{\mu_f}{\rho_f}\right)_{cold}}{\left(\frac{\mu_f}{\rho_f}\right)_{hot}} \right]^{\frac{2}{3}} \quad (9)$$

Table 1: The dimensionless parameters derived by Glicksman et al. [52], which have to be kept constant in order to achieve dynamic similarity between two different fluidized beds.

Relation	Parameters	Dimensionless number	Physical interpretation
1	$\frac{u_0^2}{gL}$	Froude number	Ratio between inertial and gravitational forces
2	$\frac{\rho_s}{\rho_f}$	-	Ratio between particle and gas inertial forces
3	$\frac{\rho_s u_0 d_p}{\mu_f}$	Particle Reynolds number	Ratio between particle inertial and fluid viscous forces
4	$\frac{\rho_f u_0 L}{\mu_f}$	Fluid Reynolds number	Ratio between fluid inertial and fluid viscous forces
5	$\frac{G_s}{\rho_s u_0}$	-	Scaled mass flux at inlet boundary
6	Bed geometry	-	Size of equipment
7	Particle size distribution	-	Particle size distribution

In order to respect dynamic similarity and thereby reflect the flow in the hot unit, a crucial parameter for the operation of fluidized beds is the pressure drop over the gas distributor. Even though this is not formally a parameter that is considered according to the work of Glicksman et al. [69], the ratio between the pressure drop over the bed and the pressure drop over the gas distributor has been shown to be of relevance for the fluidization regime established in the bed [59]. In the work conducted by Bonniol et al. [71], it was shown that additional scaling parameters that consider the pressure drop ratios over the bed and distributor should be used to complement Glicksman's scaling laws. Thus, the pressure drop ratio is also kept constant in the present work. While nozzles are used in the large-scale unit, a combination of a fine metal grid and an orifice plate is used in the cold flow models. The

pressure drop over the distributor is determined by the downscaling, while the diameter of the orifice is calculated according to the procedure of Kunii and Levenspiel [66] once the targeted pressure drop is known.

The scaling laws proposed by Glicksman et al. [69] have been experimentally verified for the fluid dynamics of the bed material using tracer experiments [52, 54, 72] and the pressure drop measurements carried out in a CFB riser [53]. An example of the similarity between the pressure drops in a large scale riser and in a fluid-dynamically downscaled (using Glicksman's simplified laws) cold flow model is shown in Figure 8 (for details, see Johnsson et al. [53]).

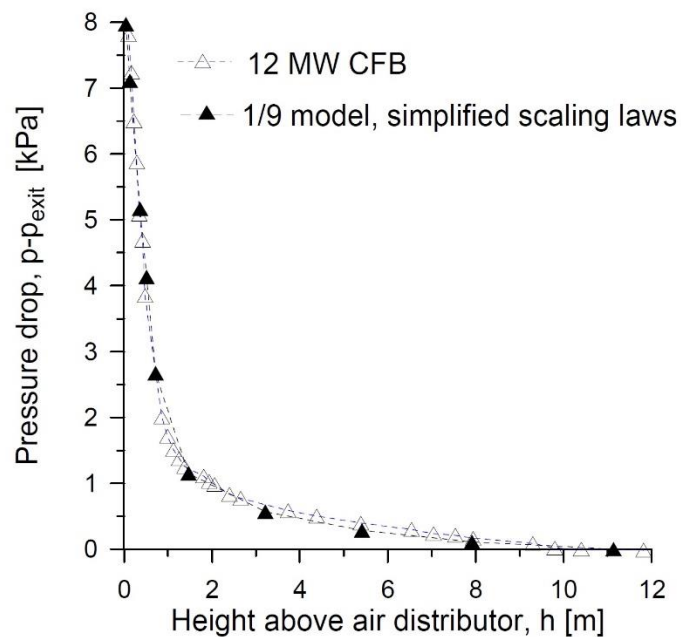


Figure 8: The similarity of the pressure drops between a large-scale boiler and a fluid-dynamically downscaled cold flow model (scale factor 1/9). Taken from Johnsson et al. [53].

Fluid-dynamic scaling of the bulk solids has been applied by several authors to characterize fluidization in various applications [63, 73, 74]. However, the use of fluid-dynamic scaling to study the mixing of fuel particles has neither been applied nor validated to date. In Paper II, an experiment is conducted to validate the method for fuel mixing and, thereafter, a large set of data is presented.

4 Experimental setup

The experimental work presented in this thesis used the four fluidized bed units shown in Figure 9, *i.e.*, three fluid-dynamically down-scaled bubbling beds operating under ambient conditions and an industrial-scale bubbling fluidized bed operating under hot conditions as a gasifier in the DFB system at Chalmers (for details, see [2, 62]). For the three down-scaled beds, Glickman's [69] full set of scaling laws was employed (see Table 1). In the design, it was assumed that either air or steam at 900°C was used in the large-scale units depending on whether combustion or gasification was investigated. From the scaling laws, the corresponding length-scale factors are computed as 1/5 or 1/6, respectively. The size of the fuel particles is also scaled using the same length-scaling factors (yielding a constant Re_p).

The cold flow model A (Figure 9a) was used in Papers I and II to investigate the lateral mixing of bed material and fuel particles in the absence of cross-flow. This model has a quadratic cross-section of 0.09 m² and is a fluid-dynamic downscale of the bottom region (the first 0.5 m above the gas distributor) of the Chalmers 12 MW_{th} FB boiler (for details of this boiler, see [75]).

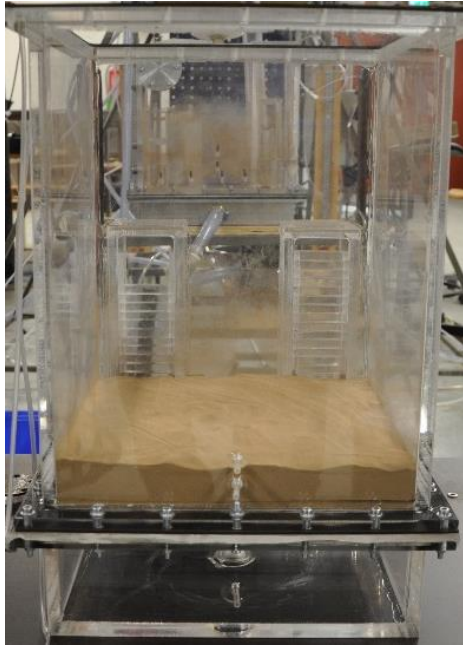
The cold flow model B (Figure 9b) was used in Paper V to study the effect of cross-flow on the lateral mixing of the fuel. This model is 0.039 m² in cross-section and is a downscale of the Chalmers 2–4¹ MW_{th} indirect gasifier [2, 62].

The cold flow model C (Figure 9c) was used in Papers III and IV, which apply 3-dimensional particle tracking experiments (one of the sensor modules for the tracking system is seen in the foreground of the photograph). This unit does not have any particular large-scale bed associated with it, and it is scaled using the assumption that it is a bed to be used in a combustion process.

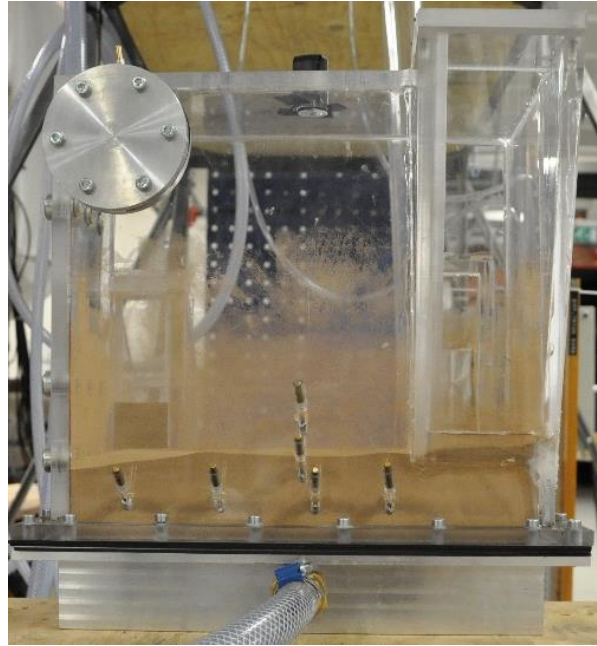
The Chalmers 2-4 MW_{th} indirect gasifier (Figure 9d) was used for the evaluation of fuel mixing at high temperature, as described in Paper VI.

The dimensions and operational conditions applied to the four beds are summarized in Table 2, where the data for the three fluid-dynamically scaled beds are presented under up-scaled conditions, *i.e.* refers to the conditions of the large-scale unit operating at high temperatures and not under the conditions of the laboratory-scale cold flow model.

¹ While the gasifier is usually operated at 2 MW_{th}, it was actually designed for operation at 4 MW_{th}.



a) Cold flow model A, bottom region of the Chalmers 12 MW_{th} boiler, used in Papers I and II.



b) Cold flow model B, downscale of the Chalmers 2–4 MW_{th} indirect gasifier, used in Paper II



c) Cold flow model C used in Papers III and IV



d) Chalmers indirect gasifier, used for the high-temperature investigation in Paper VI

Figure 9: Fluidized beds used in the experimental studies presented in the thesis.

Table 2: Summary of the dimensions and operational conditions applied to the four fluidized beds used in the present work; data are given for up-scaled conditions for cold flow models A–C. Bed D is an industrial-scale fluidized bed.

	A	B	C	D
Area (m ²)	2.25	1.44	0.72	1.44
Ratio: length to width	1	~2	1	~2
Bed height (m)	0.15–0.55	0.30	0.25–0.35	0.30
Fluidization velocity (m/s)	0.08–0.83	0.16–0.21	0.16–0.45	0.08–0.18
Fluidization medium	Air	Air	Air	Steam
Bed material	Bronze	Bronze	Bronze	Iron oxide

The relevant parameters obtained from the fluid-dynamic scaling of the systems are listed in Table 3. As a result of fluid-dynamic scaling, bronze powder was used as the bed material to maintain approximately the ratio between the gas and bulk solids densities during scaling (see Relationship 2 in Table 1). In addition to the parameters specified by Glicksman et al. [69] in the full set of scaling laws, this work also kept constant the density ratio between the bed material and fuel particles. Different fuel types were investigated, namely wood pellets, wood chips, and char from wood pellets, which scaled-down to aluminum, polyamide, and polyethylene terephthalate, respectively. For the experiments conducted with the 3D tracking system, an NdFeB permanent magnet that resembles anthracite coal was used. In Table 3 suitable densities are reported for the solids to fulfill scaling together with the densities used in this work. In the present work, the bed height was varied between 0.03 m and 0.11 m (scaling up to 0.15–0.55 m). At each bed height, several fluidization velocities were evaluated, ranging from 0.04 m/s to 0.37 m/s (scaling up to 0.08–0.83 m/s). The influence of the gas distributor pressure drop was investigated by using designs with different characteristic pressure curves while maintaining the same number and positions of the orifices.

Table 3 : Summary of the parameters for the large-scale and downscaled beds.

Parameter	Unit	Hot large-scale bed	Cold down-scaled bed; according to scaling laws	Cold down-scaled; actually used
Density, bed material	kg/m ³	2600	10600	8900
Density, char pellet	kg/m ³	400	1370	1200
Density, wood pellet	kg/m ³	950	3290	2700
Density, wood chips	kg/m ³	500	1710	1400
Density, anthracite	kg/m ³	1890	6470	7310
Density ratio (bed material / char pellet)	-	6.5	6.5	7.4
Density ratio (bed material / wood pellet)	-	2.7	2.7	3.3
Density ratio (bed material / wood chips)	-	5.2	5.2	6.4
Temperature	°C	900	20	20
Length-scaling factor, combustion	m	L_c	$L_c/5$	$L_c/5$
Length-scaling factor, gasification	m	L_g	$L_g/6$	$L_g/6$
Velocity-scaling factor, combustion	m/s	u_c	$\sqrt{u_c^2/5}$	$\sqrt{u_c^2/5}$
Velocity-scaling factor, gasification	m/s	u_g	$\sqrt{u_g^2/6}$	$\sqrt{u_g^2/6}$
Time-scaling factor, combustion	s	t_c	$\sqrt{t_c^2/5}$	$\sqrt{t_c^2/5}$
Time-scaling factor, gasification	s	t_g	$\sqrt{t_g^2/6}$	$\sqrt{t_g^2/6}$

5 Overview of available experimental methods for studying solids mixing

Different methods have been described in the literature to characterize experimentally solids mixing, an overview of which is given below (an extensive review is provided by Chaouki et al. [76]).

5.1 Tomographic methods

Tomographic methods generate a 3-dimensional reconstruction of the interior of the studied bed by combining measurements from several 2-dimensional planes. There are several different tomographic methods, and in fluidized beds, x-ray and γ -ray transmission tomography have been applied [55, 77-79]. These techniques are based on one or several radiation emitters placed on one side of the object under investigation and a single or a set of receivers placed on the opposite side. By measuring how much of the emitted radiation passes through the object to the receiver, a density distribution in the object can be back-calculated. By rotating the radiation source and receiver around the object, a 3-dimensional view is obtained. Investigators report a spatial resolution in the order of 1 mm [76]. However, since multiple scans are required at numerous angles to create a 3-dimensional view, the time resolution is limited to a period of between hours and minutes depending on the numbers of emitters and receivers used. Furthermore, since metals efficiently block x-ray and γ -ray radiation, these measurement techniques cannot be used if fluid-dynamic downscaling is applied. The equipment required for x-ray and γ -ray tomography is typically very expensive and there are obvious safety concerns associated with ionizing radiation [80]. A schematic of the two types of tomographic setup is given in Figure 10.

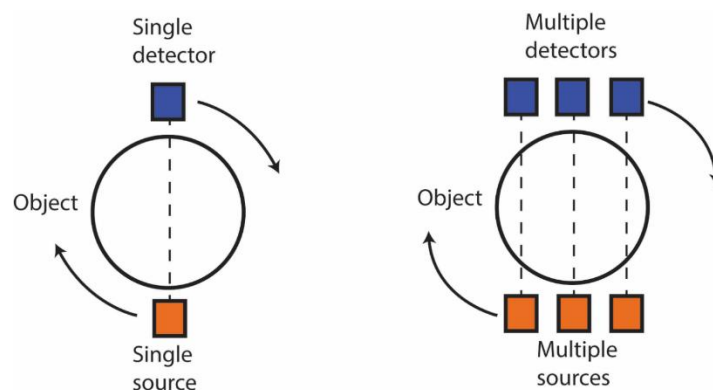


Figure 10: Illustration of the principles of x-ray and γ -ray transmission tomography.

Electrical impedance tomography is based on measuring the electrical properties, such as capacitance, resistance or inductance, in the medium of the studied object. If the medium conducts electricity, resistance or inductance measurements can be applied, whereas for an insulating medium, such as a fluidized bed, capacitance measurements can be used [76]. Electrical capacitance tomography (ECT) has been applied to fluidized beds by several

investigators [81-84]. The ECT works by building up an electrical charge in one of the sensors at a time while measuring the electrical field with other sensors, and thereafter alternating the sensor that builds up the electric charge. Since the capacitance (the amount of charge that a sensor can hold) is dependent upon the size of the sensor, higher accuracy is achieved with larger sensors [85]. In contrast, the spatial resolution is determined by the number of sensors, and the number of independent measurements are given by: $N(N-1)/2$ where N is the number of sensors. Thus, there is a tradeoff between the spatial resolution and accuracy as only a certain amount of space is available for placement of the sensors around the object of the investigation. As most studies use either 8 or 12 sensors, resulting in an image that contains either 28 or 66 pixels, the spatial resolution of ECT is very limited. However, the sampling frequency is high; investigators have reported sampling frequencies of up to 400 Hz [86]. ECT has been used in industrial applications and should work with the metallic bed materials used in fluid dynamic downscaling. A schematic of an ECT system is given in Figure 11, where one of the sensors is charged and the other sensors are measuring the electrical field (indicated by dashed lines); the electric field is symmetric so only half of it is depicted.

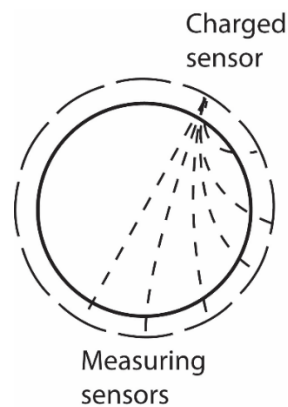


Figure 11: Schematic of the electrical capacitance tomography (ECT) system.

Since the present work applies fluid dynamic downscaling metallic bed material is used (since ambient air is the fluidization medium), thus x-ray and γ -ray tomography cannot be used due to the short distances such rays can penetrate. Since the ECT method allow provides low spatial resolution it is not suitable either for the purpose of this work.

5.2 Particle tracking methods

Several methods are available for tracking a single particle in fluidized beds. While these methods are not tomographic, they can provide information about flow structures and particle concentrations. Positron emission particle tracking (PEPT) is based on tracking positron-emitting particles that have been activated in a cyclotron or are naturally radioactive [87, 88]. When a positron collides with an electron the two particles are annihilated and two γ -rays are emitted back-to-back. Using detectors similar to those employed for γ -ray tomography, the location of the particle collision, *i.e.* the location of the tracer, can be

calculated. With PEPT, 3-dimensional information about the tracer trajectory is obtained to a precision of 5 mm, with a sampling frequency of 50 Hz [89]. The safety requirements for PEPT are higher than those for x-ray and γ -ray tomography, since the tracer particles are continuously emitting positrons, whereas the ray-based systems are only emitting during the period that the equipment is operational [76].

Radioactive particle tracking (RPT) is similar to PEPT but instead of positron emission the tracer particle typically emits γ -rays directly. RPT was first applied to fluidized beds in 1964 by Kondukov et al. [90]. However, due to the limited data processing capability at the time, no quantitative information was obtained. More recent investigations using RPT [12, 91, 92] have acquired quantitative 3-dimensional information regarding tracer flow fields in fluidized beds. RPT has been reported as having spatial resolution of 7 mm and sampling frequency of 100 Hz [93]. As with the other methods in which γ -rays are used, RPT is not applicable to fluidized beds that have a metallic powder as the bed material.

Optical methods for particle tracking have been applied in several studies. In pseudo-2-dimensional cold flow units with a transparent wall, a continuous particle trajectory can be detected, and modern cameras can provide high spatial and temporal resolutions (see Table 4) [40, 49, 94]. However, the flow is naturally confined in a pseudo-2-dimensional system, which establishes solids patterns with wall effects, so it is not necessarily representative of 3-dimensional units. Some authors [39, 45] have applied optical methods to the bed surface of a 3-dimensional bed under cold flow conditions and shown that the particle trajectory is not continuous, as the tracer may become immersed in the dense bed, such that long video recordings are required to obtain statistically robust information about the mixing of the tracer (for further details of these methods, see Paper II). This thesis contributes to the development of optical methods by showing how it is possible to measure particle trajectories in industrial-scale fluidized beds operated at high temperatures. Paper VI demonstrates such a method, in showing that camera calibration enables a spatial resolution of 0.8 mm at a frame rate of 30 frames per second.

Magnetic particle tracking (MPT), which is a relatively recent development, has been used by several investigators [47, 95-98]. The MPT method tracks the magnetic field surrounding a permanent magnet, yielding not only the position of the magnetic tracer but also its orientation; this combination of information is not provided by any of the aforementioned techniques. As the magnetic field is not blocked by metallic powders, MPT can be used in fluid-dynamically downscaled beds provided that a non-magnetic bed material is used. In Paper III, it is shown that the spatial resolution is approximately 1 mm and that temporal resolutions in the order of milliseconds can be achieved with MPT. In Paper IV, it is shown that time for processing the raw measurements can be reduced significantly. The drawbacks of MPT are that it cannot be applied to units that are operated at high temperatures and that the distance

from the tracer particle to the detector is limited to 0.3 m (for magnets with sizes chosen according to the fluid-dynamical down-scale of a typical solid fuel in a fluidized bed).

Similarly to what was mentioned for the tomographic methods RPT is ruled out because of its inability to penetrate far in the metallic bed material. Therefore optical and MPT methods are suitable and these are applied in the present work,

A summary of the abovementioned tomographic and particle tracking techniques is given in Table 4.

Table 4: Measurement techniques used in investigations of solids mixing in fluidized beds.

Technique	Tomographic	2D/3D	Resolution	Fluid dynamic scaling	Other	Ref.
x-ray/ γ -ray	Yes	3D	1 mm, minutes to hours	No	Safety issues	[55, 77-79]
ECT	Yes	3D	Several centimeters, 0.003 s	No		[81-84]
PEPT	No	3D	5 mm, 0.02 s	No	Safety issues	[87, 88]
RPT	No	3D	7 mm, 0.01 s	No	Safety issues	[12, 91, 92]
Optical	No	2D	<1 mm, 0.03 s or better	Yes		[40, 45, 49, 94]
MPT	No	3D	1 mm, 0.001 s	Yes		[47, 95-98]

Optical methods are used in Papers II and VI and MPT is used in Papers III and IV.

6 Data evaluation

The data obtained with the optical and MPT methods mentioned in the previous section need some processing before the results can be extracted, this processing is described in this section. The methods applied in this thesis to evaluate the lateral mixing of solids can be classified as either *indirect* or *direct*. Each of these methods yield distinct types of information and entail different data evaluation methods, as presented below. Furthermore, Kalman filtering is applied to the trajectory data obtained in Papers III and IV to reduce the influence of measurement noise, as well as to the data in Paper VI to allow the simultaneous tracking of multiple particles, as explained briefly below. Finally, a multivariate data analysis method called principal component analysis (PCA) is applied to uncover trends among the operational parameters applied and the lateral dispersion coefficients for both the bed material and the different fuel types investigated.

6.1 Indirect methods

When the indirect method is applied, a batch of tracer material is fed at one corner of the bed and samples are collected over time at intervals of a few seconds. This yields a residence time distribution within the reactor [99-101]. By solving the transient transport equation (*e.g.*, Eqns. (1), (3) or (4)) and comparing the results to the measurements, the concentration field in the reactor can be obtained. In the present work (Paper I), a mixture of bronze powder and iron powder is used to evaluate mixing of the bed material, whereby the iron powder can be separated magnetically to allow quantification of the tracer concentration in each sample. For evaluation of the mixing of fuel particles, it is sufficient to count the number of fuel tracer particles collected in each sample.

An example of a measured concentration profile and the fitted solutions of Eq. (1) is given in Figure 12 for a case without solids cross-flow. The outlet tracer concentration plateaus when the bed becomes well-mixed. If a solids cross-flow is present in the system, the tracer concentration decreases after peaking, owing to the dilution effect of the bulk cross-flow.

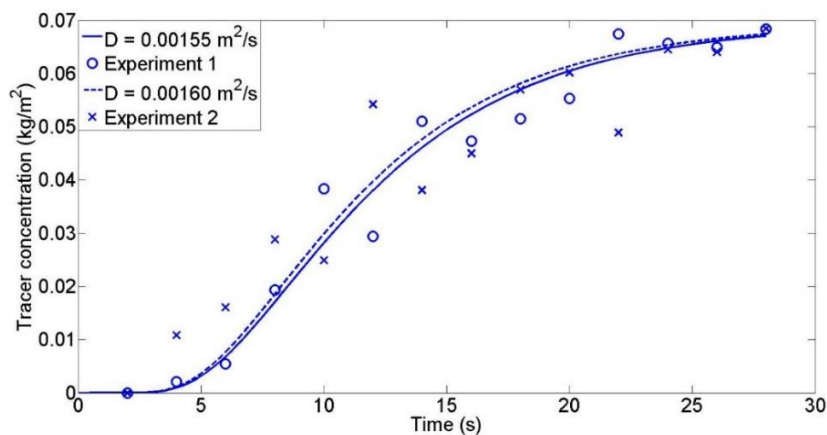


Figure 12: Typical tracer concentration profile for a case in which the indirect method is used in the absence of solids cross-flow. Values are shown on a downscaled basis. Taken from Paper I.

6.2 Direct methods

Direct methods provide information about the location of the tracer particles at different time-points. Thus, there is no need to collect samples of the tracer particles. In the present work, the optical and MPT methods are applied in a direct fashion.

Papers II and VI apply optical methods to track tracer particles by recording their movements with a video camera. By coating the tracer particles with different fluorescent markers (colors), multiple particles can be tracked simultaneously using the direct method when applied to a cold flow model, as shown in Paper II. In Paper VI, the tracking of multiple particles was applied to biomass in an industrial-scale bed. Since the video camera is mounted above the bed, this method can only detect particles as they emerge at the bed surface.

The lateral dispersion coefficient is evaluated from the tracer particle positions using Einstein's equation for Brownian motion, Eq. (10), where Δt is the time between two particle detections and ΔL is the distance traveled by the particles between detection events.

$$D = \frac{\Delta L^2}{2\Delta t} \quad (10)$$

Since the dispersion approach is valid on a macroscopic scale, particle movements that are too small have to be filtered out before the dispersion coefficient can be determined with Eq. (10). Thus, the algorithm shown in schematic in Figure 13 is used to remove the particle movements that occur within the same mixing cell. Such movements are not contributing effectively to the macroscopic lateral mixing described by the dispersion coefficient. In Figure 13, a particle has been detected at the locations indicated by the solid black dots, and the dashed arrows indicate the movement of the particles between two consecutive particle detections. A thin solid arrow is used to indicate when a particle moves to a different mixing cell. However, it is only the distance and elapsed time to the first detection event in a new mixing cell that are relevant in the evaluation; these are marked with thick solid arrows.

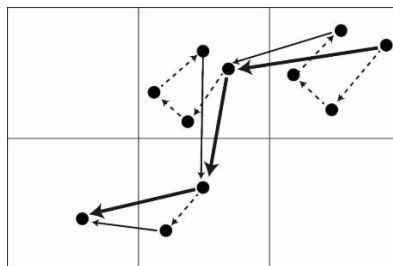


Figure 13: The algorithm used in the direct method filters out particle movements that are too small to contribute effectively to the macroscopic mixing, which is described by dispersion. Taken from Paper II.

6.3 Kalman filtering

In applications used for tracking moving targets (*e.g.*, tracking airplanes with radar or position estimation using GPS), it is common to improve tracking the estimation of the tracer particle position (and velocity) by applying a Kalman filter [102, 103], whereby the measurements are combined with a model so as to reduce measurement uncertainties. The model used is based on Newton's laws of motion, wherein the second derivative of the tracer particle position (*i.e.* acceleration) is related to the forces acting on the tracer particle. Since sampled data are used, the differential equations need to be discretized, resulting in the following state-space formulation:

$$\mathbf{x}^{k+1} = \mathbf{F}\mathbf{x}^k + \mathbf{w}^k \quad (11)$$

$$\mathbf{y}^k = \mathbf{H}\mathbf{x}^k + \mathbf{v}^k \quad (12)$$

where the matrix, F , contains a linear model of the physics, and H is a matrix that relates the estimated states to the actual measurements. Furthermore, Gaussian noise is added to both the model and the measurements by means of the vectors w and v , respectively. The noise vectors w and v have covariance matrices Q and R , respectively. The state vector is iteratively updated through a *prediction step* (taking into account the model) and a *correction step* (accounting for measurements). In these two steps, both the state vector and a covariance matrix are updated through a number of matrix vector operations.

Prediction step	
Predicted (<i>a priori</i>) state estimate	$\hat{\mathbf{x}}_{k k-1} = F\hat{\mathbf{x}}_{k-1 k-1}$
Predicted (<i>a priori</i>) estimated covariance	$P_{k k-1} = FP_{k-1 k-1}F^T + Q$
Correction step	
Measurement residual	$y_k = z_k - H\hat{\mathbf{x}}_{k k-1}$
Residual covariance	$S_k = HP_{k k-1}H^T + R$
Kalman gain	$K_k = P_{k k-1}H^T S_k^{-1}$
Updated (<i>a posteriori</i>) state estimate	$\hat{\mathbf{x}}_{k k} = \hat{\mathbf{x}}_{k k-1} + K_k y_k$
Updated (<i>a posteriori</i>) estimated covariance	$P_{k k} = (I - K_k H)P_{k k-1}$

Where z is a vector contains the measurements.

6.4 Principal component analysis

In the experiments conducted for this thesis, fluidization velocity, bed height, and gas distributor are the parameters that are varied in order to study their influences on the resulting output parameters. The outputs evaluated in this thesis are the lateral dispersion coefficients (for bed material and three fuel types), mixing cell size, and pressure fluctuations. As several of these parameters are coupled, it is difficult to visualize the trends in the data, and many dimensions would be required in the plots. To overcome this obstacle, multivariate data analysis is used, in particular the technique called principal component analysis (PCA) [104]. Using PCA, the dimensionality of the data is reduced by projecting the data to a subspace of lower dimensionality, while maximizing the variation in the data. Thus, it is possible to discover trends and patterns in the original data and present them in a 2D or 3D graph. An example of PCA is shown in Figure 14, where a 2-dimensional dataset is projected onto a line (1D data). PCA chooses the line that captures the maximum variation of the data and assigns to it the first principal component. The line chosen by the PCA algorithm is a linear combination of the original variables; a physical interpretation of this line is not straightforward as it combines several parameters. When PCA is used, the projection is made orthogonal to the line, in contrast to the least-squares method, which only considers the vertical direction, as indicated in Figure 14.

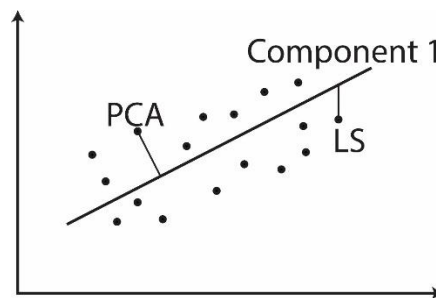


Figure 14: The data shown are 2-dimensional but can be projected onto the 1D line without too much loss of information. The line shown in the figure is the first principal component. When PCA is used, the projection is made orthogonal to the line, as opposed to least-squares (LS), which projects in the vertical direction only.

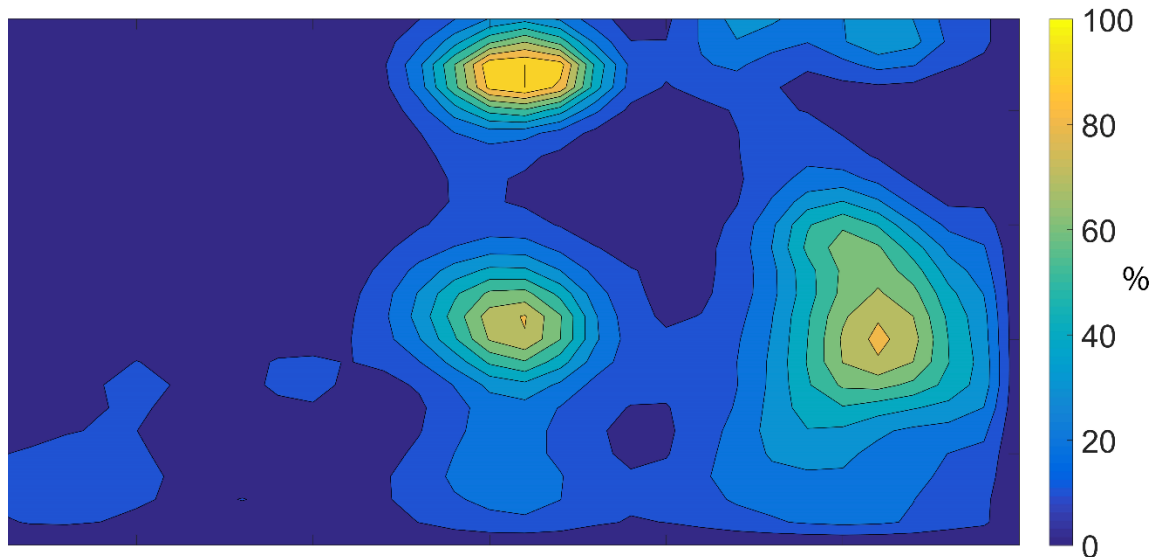
When performing PCA, two sets of data are obtained and these are referred to as ‘scores’ and ‘loadings’. The scores are the representation of the original data-points in the reduced dimensional space. Thus, when the data-points in Figure 14 are projected onto the line the locations on the line become the scores. Data-points that are located in proximity to each other are similar, and the loadings explain what makes the data-points similar. The loadings also give an indication of what proportion of the original variables is present in each principal component.

7 Results

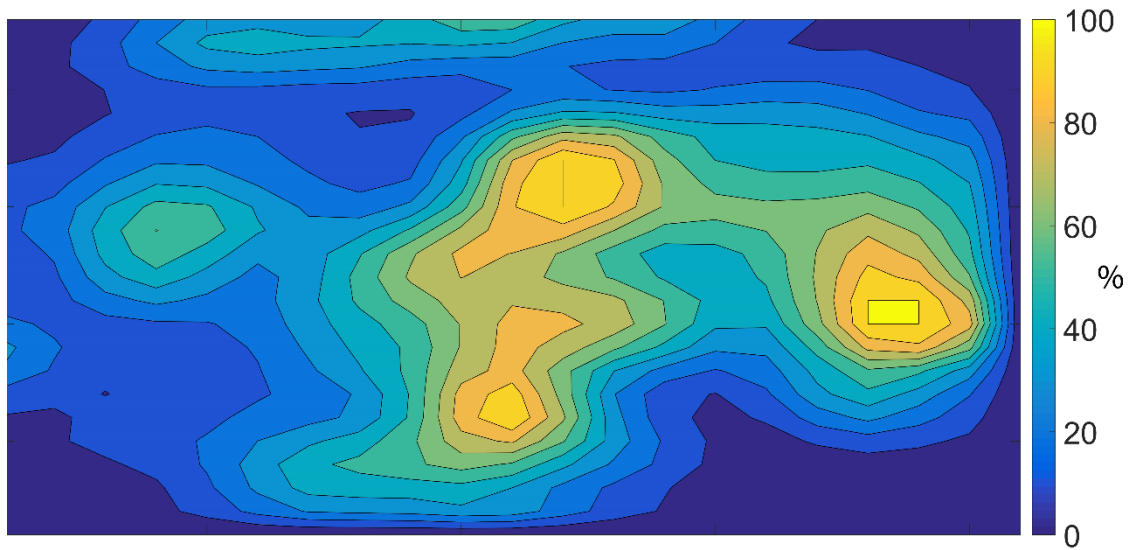
In this section, the main results from the six papers of this thesis are summarized and the connections between the papers are elaborated. The section starts with the confirmation of the existence of mixing cells in 3-dimensional beds, which is the basis for the dispersive mixing assumption. Next, the dispersive model is applied and the dispersion coefficients are evaluated. Finally, the influence of bulk solids cross-flow on the mixing of fuel particles is considered.

7.1 Existence of mixing cells

As mentioned in Section 2.2, mixing cells have been observed in 2-dimensional beds [40]. In Paper VI, the movement of fuel particles on the surface of an industrial-scale fluidized bed was analyzed, revealing that similar patterns of fuel-rich and fuel-lean regions occur in the absence of cross-flow, as shown in Figure 15a. This indicates the existence of mixing cells in large-scale fluidized beds. The regions with low concentrations of fuel particles correspond to regions where the gas bubbles emerge, and the regions with high concentrations of fuel particles correspond to the regions where the particles sink. Thus, mixing cells can be observed by evaluating the fuel concentration at the bed surface, as shown previously by Olsson et al. [39]. However, when a cross-flow is present the mixing cells are less well-defined and the convective contribution of the cross-flow influences the mixing cells (Figure 15b). The existence of mixing cells within 3-dimensional beds is further explored by applying the MPT technique to a fluid-dynamically downscaled bed (Figure 16).



a)



b)

Figure 15: Localization of fuel particles at the surface of an industrial-scale fluidized bed: a) in the absence of cross-flow b) in the presence of cross-flow.

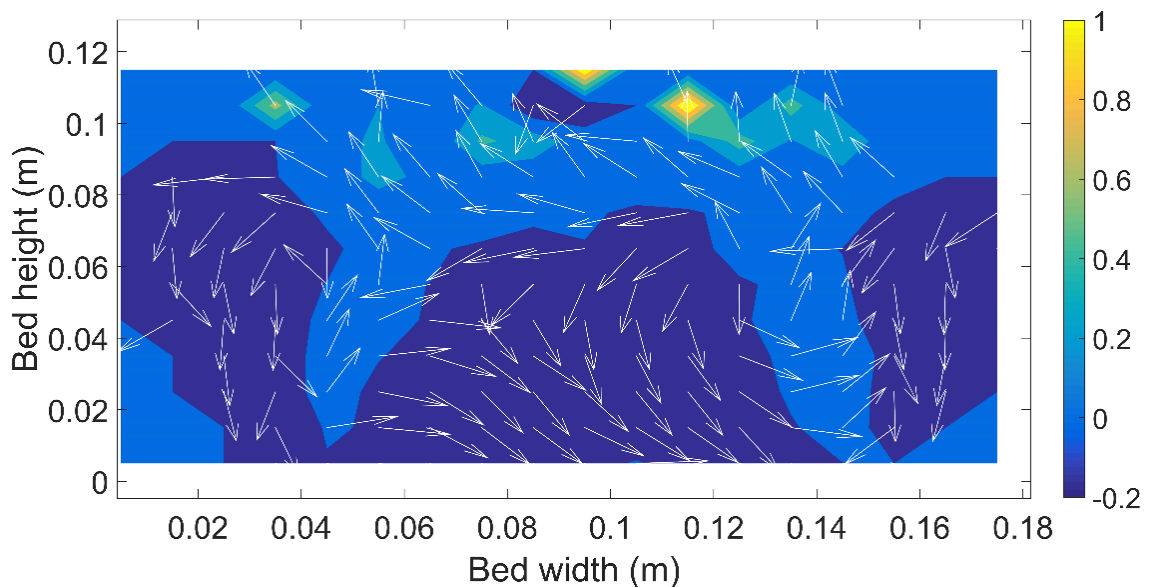


Figure 16: Analysis of slices from a 3-dimensional bed using MPT reveals flow patterns consistent with mixing cells. Taken from Paper IV.

Using the MPT technique, the mixing cells were observed to increase moderately in size with increasing gas velocity, whereas no clear trend was seen when the bed height was varied, probably due to the limited range of bed heights used in the MPT tests. However, when a wider bed was used in Paper II, visual inspection revealed that the mixing cells grew approximately linearly with the bed height. Papers II and IV both show that greater drops in pressure over the gas distributor increased the sensitivity of mixing cell size to the operational

parameters. This may be explained by the fact that in low-pressure-drop distributors, more gas passes the bed as a through-flow rather than in the form of visible bubbles. Preliminary results indicate that the mixing cell size, L_{cell} , in Eq. (2) can roughly be described as a linear function of bed height, h , as follows:

$$L_{cell} = a \cdot h + b \quad (13)$$

where the intercept, b , is dependent upon the gas distributor characteristics. However, further investigations are needed to confirm these results.

The change that occurs in the mixing cell size with operational conditions is one of the reasons for the observed difference in behavior between the lateral dispersion coefficients and the bubble mixing factors. While the lateral dispersion coefficients increased with both gas velocity and bed height, the trends for bubble mixing factors were less clear. In Paper I, we report that for the bed material, the bubble mixing factor increased with the gas velocity but was essentially independent of the bed height. In Paper II it was found for all the investigated fuel types that the bubble mixing factor was independent of the gas velocity when a low-pressure-drop distributor was used. For the high-pressure-drop distributor, the bubble mixing factor increased with the gas velocity for char and pellets but not for wood chips.

The existence of mixing cells in 3-dimensional beds and beds operated at high temperatures justifies the use of dispersive models for describing the bubble-induced mixing of solids. However, such models require dispersion coefficients, which will be considered in the following sections.

7.2 Lateral dispersion without cross-flow

The lateral dispersion of bed material was found to increase with both fluidization velocity and bed height, and the influences of the operational parameters became more pronounced when a high-pressure-drop distributor was used. The dispersion coefficients listed in Paper I are one to two orders of magnitude larger than the values presented previously in the literature, possibly due to the fact that the data in the literature are derived from small units (in which wall effects are of greater significance) without employing fluid-dynamic scaling.

When the data from the bed material experiments were evaluated using PCA (an analysis that is not presented in Paper I), deeper knowledge of the fluid-dynamics was gained. The loadings from the PCA are shown in Figure 17, and with the use of three principal components, 93 % of the variation of the data is explained. The lateral dispersion of bed material was clearly coupled to the flow of gas bubbles, as evidenced from the amplitude of the pressure fluctuations and the finding that the dispersion coefficient loadings being located in proximity

to each other. As expected, the amplitude of the pressure fluctuations increased with increases in bed height, due to bubble coalescence. As the bubbles coalesced, the number of bubbles decreased, so the characteristic frequency of the bed decreased. As shown in Figure 17, the amplitude and frequency are negatively correlated. In the same figure, it is clear that the lateral dispersion coefficient is increasing with the gas velocity.

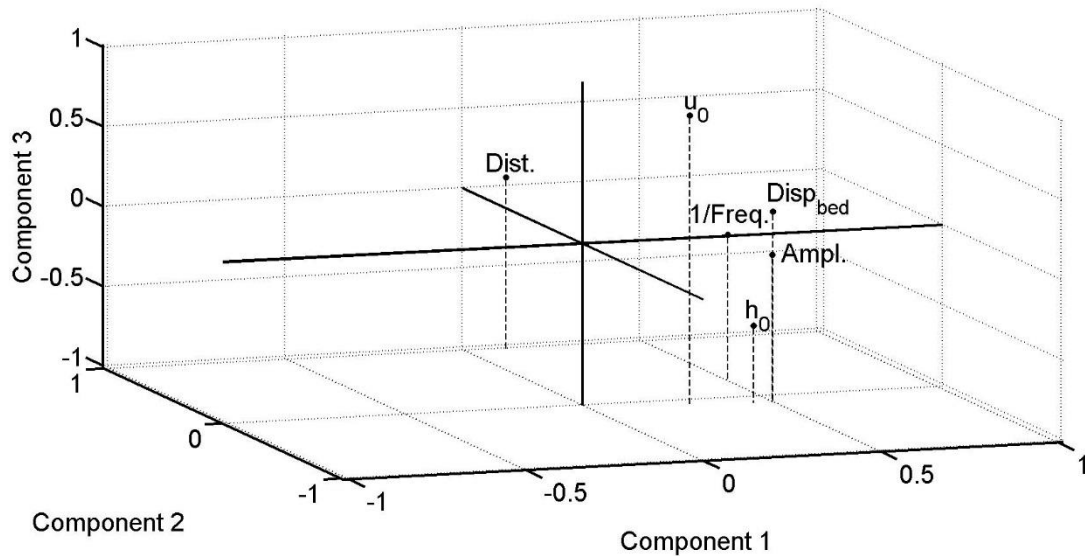


Figure 17: PCA of the data obtained for bed material mixing. The dispersion coefficient for the bed material is coupled to the flow of gas bubbles.

For the lateral dispersion of fuel, the application of fluid-dynamic scaling laws was validated initially, which was not done previously in the literature. This validation was based on an experiment that was conducted in cold flow model A, resembling the investigation of Niklasson et al. [37] in which fuel mixing was investigated in a large-scale boiler operated under hot conditions. As shown in Figure 18, the use of fluid-dynamic scaling yields a lateral dispersion coefficient similar to that measured by Niklasson et al. [37] at a larger scale. It is also worth noting the considerable variability in the complementary literature data (Figure 18), which range across several orders of magnitude. For cases where the same bed is used the variation in the measured lateral dispersion coefficient is explained by varying operational conditions. However, there is a trend seen in Figure 18 that the lateral dispersion coefficient increases with the bed size. This is explained by the stronger influence of wall effects observed in small-scale equipment, which reduces solids dispersion. It is also noteworthy that when Olsson et al. [39] investigated lateral dispersion under cold conditions in a large-scale unit of approximately the same size as the unit used by Niklasson et al. [37], the resulting dispersion coefficient was two orders of magnitude lower than the value derived by Niklasson et al. [37]. Therefore, when studying solids mixing, it is important to consider the effects of both temperature and bed size.

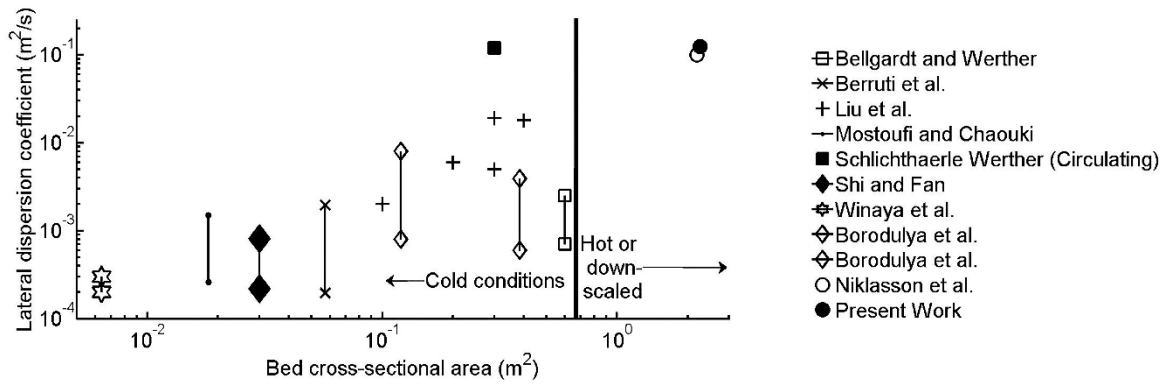


Figure 18: Comparison of data from the literature regarding lateral dispersion coefficients. The present work employs fluid-dynamic scaling to resemble the large-scale hot case reported in Niklasson et al. [37]. The data plotted with ranges indicated that operational conditions were varied in the investigation. Values are shown on an up-scaled basis. Data taken from [18, 19, 24, 30, 31, 35, 37, 43, 45, 105]. Figure taken from Paper II.

Using PCA of the data presented in Papers I and II, it is possible to evaluate the influence of bed material mixing on the mixing of fuel particles, in addition to the influence of the operational parameters alone. Figure 19 shows the PCA of the data; with three principal – components, 94% of the variation in the data is explained. The lateral dispersion coefficients for the pellets, wood chips, and bed material are strongly correlated, as their loadings are located in almost the same place. In contrast, the lateral dispersion of char is not as heavily influenced by the bed material mixing, as the point D_{char} is not clustered with D_{bed} . Char is the particle type with the lowest density of all those studied. Therefore, it is not unexpected to see a different mixing behavior for this particle type.

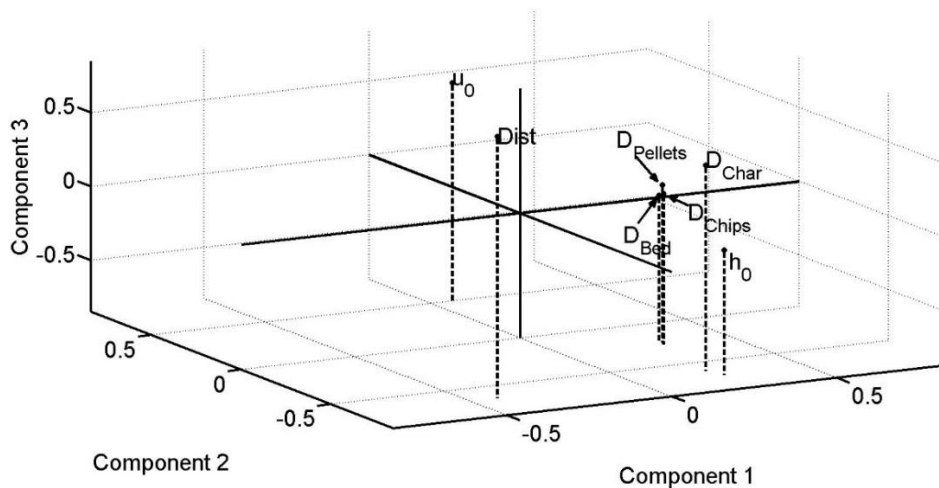


Figure 19: PCA of the data presented in Papers 1 and 2 shows a strong correlation between pellets, wood chips, and bed material. The lateral dispersion of char particles is mainly influenced by the pressure drop over the gas distributor. Taken from Paper II.

7.3 Solids mixing with cross-flow

As mentioned above, the lateral mixing of pellets is coupled to that of the bed material. However, in the previous discussion, only the bubble-induced, dispersive bulk mixing in a stationary bubbling bed was considered. When a solids cross-flow is present through the bed a second mixing mechanism, which is convective in type, must be considered. In Paper V, it is shown that a 2-dimensional convection-diffusion equation can be used to describe the mixing of fuel particles when a cross-flow is present. A method for estimating the velocity field using the potential flow theory yields a reasonable velocity field at low computational cost. An alternative approach is to apply the method of Kobayashi et al. [21] (and references therein), solving the Navier-Stokes equations for a single-phase flow. Kobayashi et al. investigated convective transport in the vertical direction of dense bottom beds; this is now applied to the lateral direction instead. Kobayashi et al. used values for the apparent viscosity in the range of 0.2–1.0 Pa·s. Estimating the lateral velocity field using this method gives the results shown in Figure 20, where the colors indicate the velocity in m/s. Here, a value of 1.0 Pa·s is used for the apparent viscosity, although additional investigations are needed to establish an accurate value. It should be noted that the shape of the velocity field differs from that obtained using potential flow, and that there is now a region to the left of the inlet where the velocities are very low; a feature that is not captured by potential flow. Manual inspection of the videos taken in the Chalmers gasifier reveals that the fuel particles have a tendency to accumulate and move slowly in the region where low velocities are predicted. If the time and computational resources allows to solve the Navier-Stokes equations the approach based on the findings of Kobayashi et al. is feasible. However, this was not elaborated in Paper V because one of the goals was to propose a method which gives reasonable results at minimum computational effort.

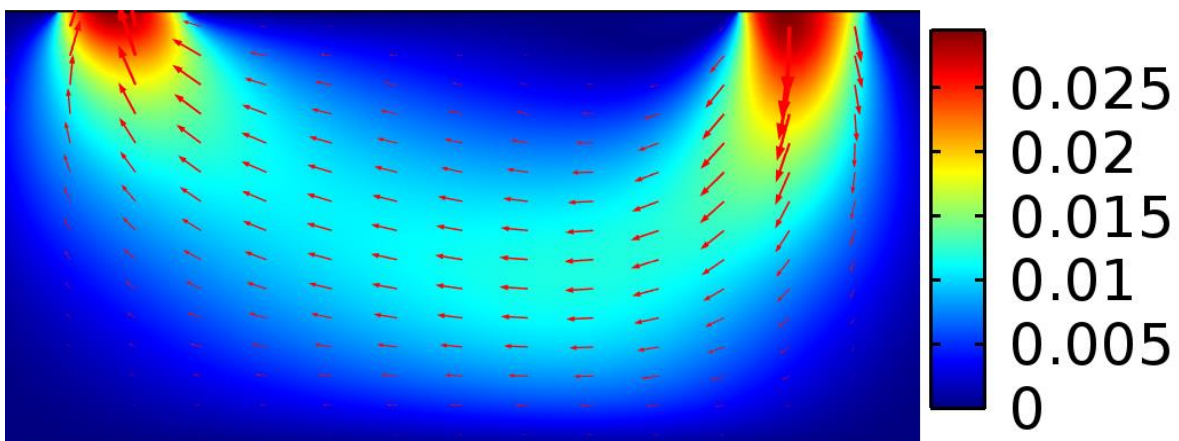


Figure 20: Alternative simulation of the velocity field induced by solids cross-flow. The apparent viscosity is 1.0 Pa·s. The color map shows the magnitude of the velocity in m/s.

In Paper V, it is shown that there is a certain slip between the bed material and fuel particles, which has not previously been investigated. In Figure 21, this slip of fuel particles with respect to the bulk cross-flow is quantified using a cross-flow impact factor, θ . A value for θ of zero

means that the fuel does not follow the flow of bed material (full slip) and a value of 1 indicates that the fuel and bed material attain the same velocity (no slip). The cross-flow impact factor is evaluated experimentally by fitting the measured tracer concentration (sampled at the outlet after a batch of tracer particles were added to the fluidized bed) to Eq. (3).

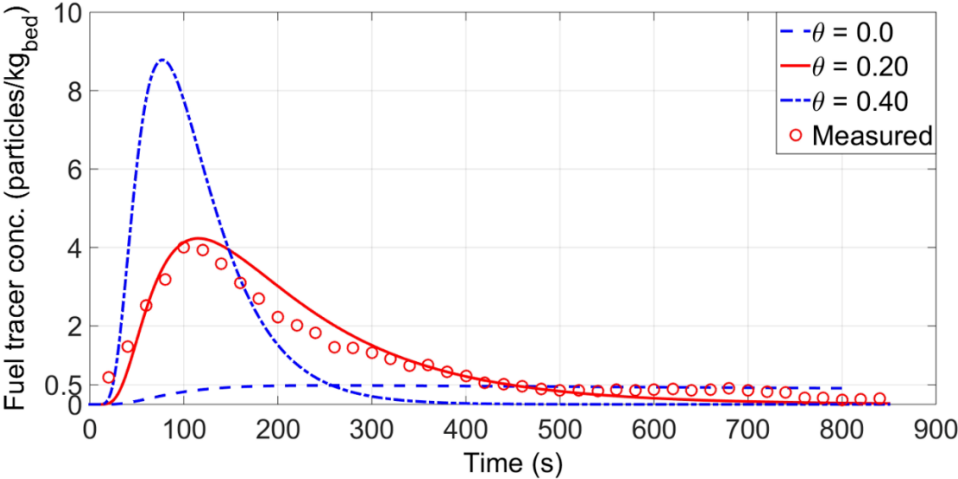
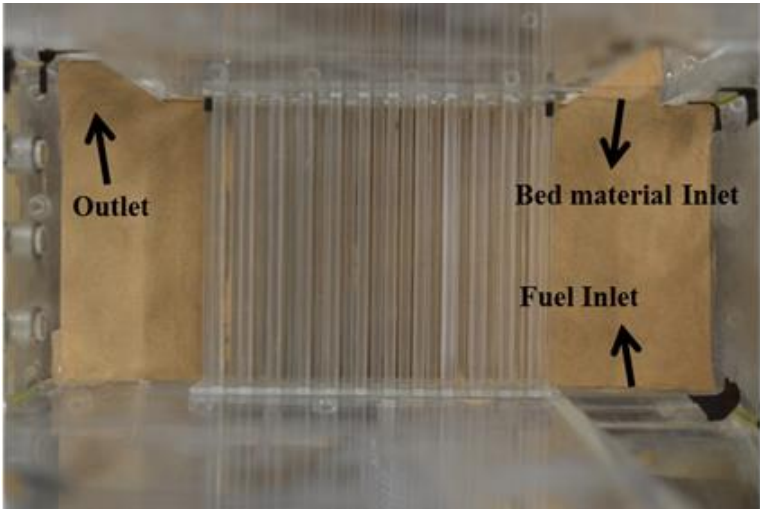
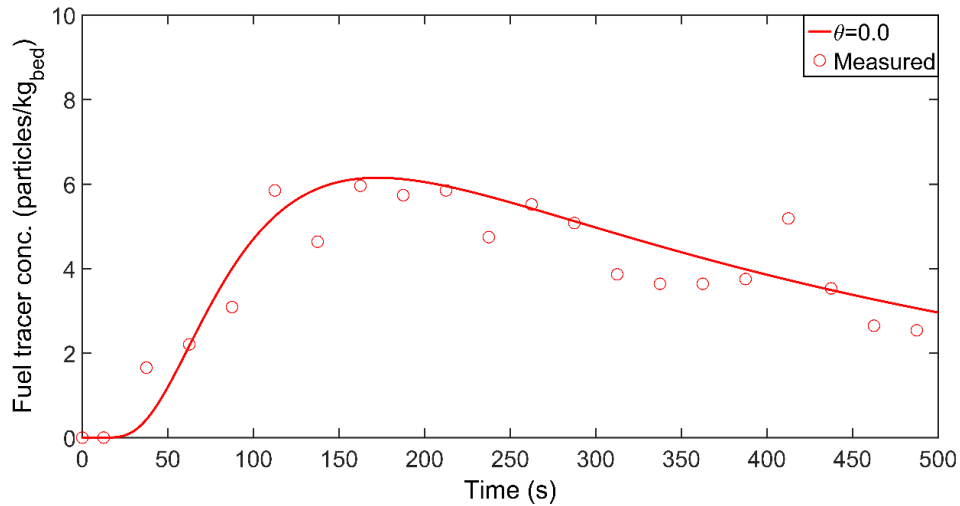


Figure 21: The presence of a solids cross-flow through the bed influences the lateral mixing of the fuel, as indicated by the impact factor θ . The values are shown on a down-scaled basis. Taken from Paper V.

In DFB systems for indirect gasification, it may be relevant to increase the residence time of the fuel particles while maintaining a large cross-flow of bed material, which provides the heat for endothermic reactions. In an attempt to decouple the fuel particles from the flow of bed material, a tube bundle was inserted into cold flow model B, as shown in Figure 22a [38]. When the cross-flow impact factor is fitted to the measurements (presented in Figure 22b) using Eq. (3), it becomes zero, which indicates that the lateral mixing of fuel is decoupled from the convective flow of the bed material.





b)

Figure 22: The mixing of fuel particles is decoupled from that of the bed material by inserting a tube bundle. a) The location of the tube bundle in cold flow model B, as viewed from above. b) The results of the experiment show that decoupling has been achieved.

In Paper VI, the influence of cross-flow on fuel mixing in an industrial-scale bed was investigated. It is shown that the lateral velocity of the fuel particles increases with the cross-flow (Figure 23). Furthermore, the investigation in Paper VI shows that an increased cross-flow reduces the vertical mixing of the fuel. This is evident in Figure 24, where a high mixing index, X_{mix} , indicates a well-mixed bed. In Paper VI, the influence of fuel density was also investigated; it is shown that lighter particles yield higher lateral velocities due to their lower inertia.

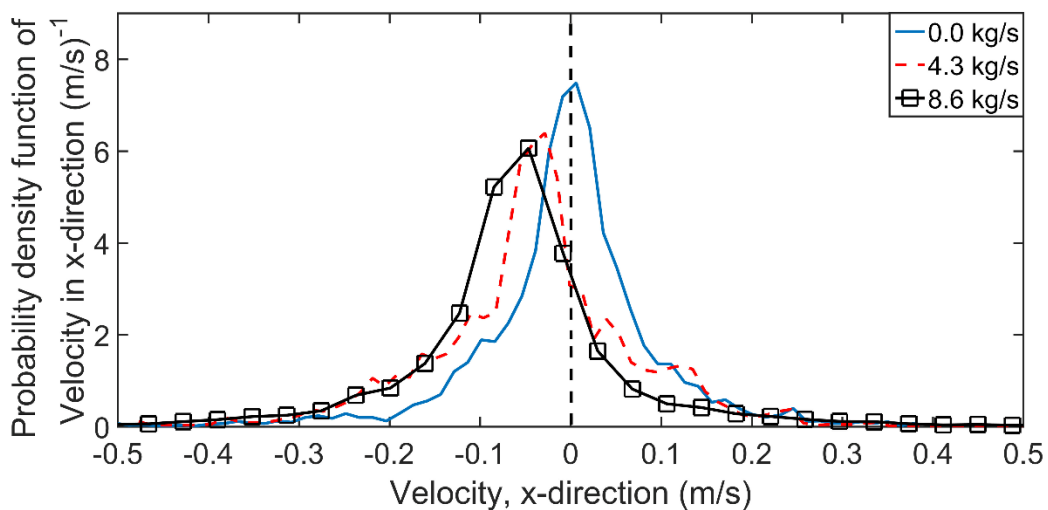


Figure 23: The influence of cross-flow on the lateral velocity of the fuel (pellets). Increases in the cross-flow shift the distributions to the left, indicating a convective mixing mechanism. Taken from Paper VI.

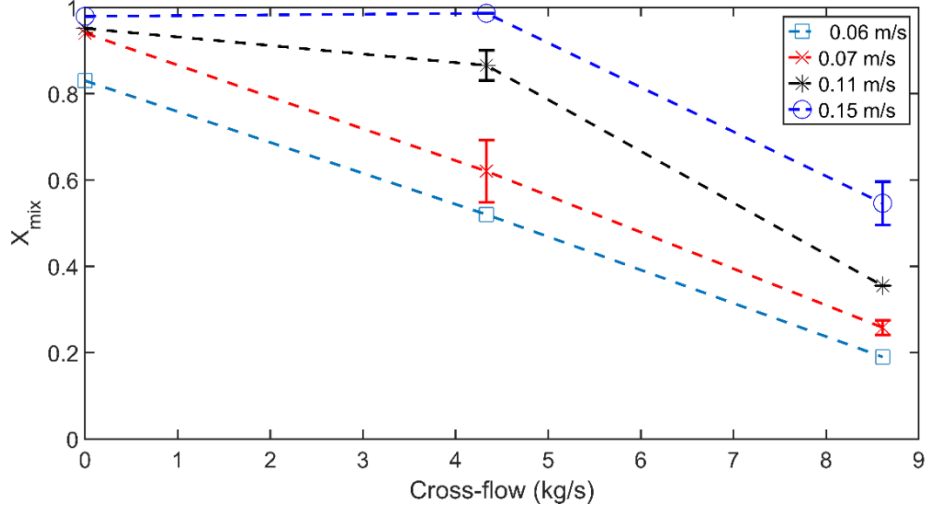


Figure 24: Vertical mixing (quantified with a mixing index, X_{mix}) is reduced when the cross-flow is increasing. Error bars are included for the measurements, which were repeated. Taken from Paper VI.

7.4 Pyrolysis time of fuel particles

In Paper VI, the time period over which it is possible to track a batch of fuel particles is limited to 60–70 seconds before the particles become no longer visible. This time can be compared to the time of pyrolysis of the fuel particles, which is assessed by abruptly terminating the fuel feeding during steady-state operation and measuring the pyrolysis components, such as methane, (y), with an online instrument. This procedure was applied by Larsson [106] and is used in the present work to quantify the pyrolysis time of the fuel particles in the Chalmers indirect gasifier. Since the gas analyzer is located far away from the devolatilizing fuel particles, the gas mixing and transport delay need to be accounted for when studying the transient data provided by the gas analyzer. This was achieved by shutting off the flow of the purge gas, *i.e.*, the dry flue gas, to the cell feeders and monitoring the change in CO_2 concentration, which yields a step response, (h_{step}). The measured methane concentration (y) is a convolution between the impulse response of the gas mixing and transport delay ($h_{impulse}$) and the methane concentration leaving the devolatilizing particles (x), according to Eq. (14):

$$y(t) = \int_0^t x(\tau) h_{impulse}(t - \tau) d\tau \quad (14)$$

where the impulse response ($h_{impulse}$) is the time derivative of the measured step response (h_{step}). The concentration of methane at the bed surface is obtained by solving Eq. (14) for (x). Since convolution in the time domain corresponds to multiplication in the Fourier domain, the deconvolution of Eq. (14) can be performed in the Fourier domain according to Eq. (15), where the Fourier transform and its inverse are represented by F and F^{-1} , respectively.

$$x(t) = F^{-1} \left\{ \frac{F\{y(t)\}}{F\{h_{impulse}(t - \tau)\}} \right\} \quad (15)$$

Deconvolution is an ill-posed problem [107], so noise in the measurements distorts the analysis. In the present work, a function is fitted to the measured data to reduce the influence of measurement noise and the subsequent deconvolution is applied to the fitted curve (see Figure 25).

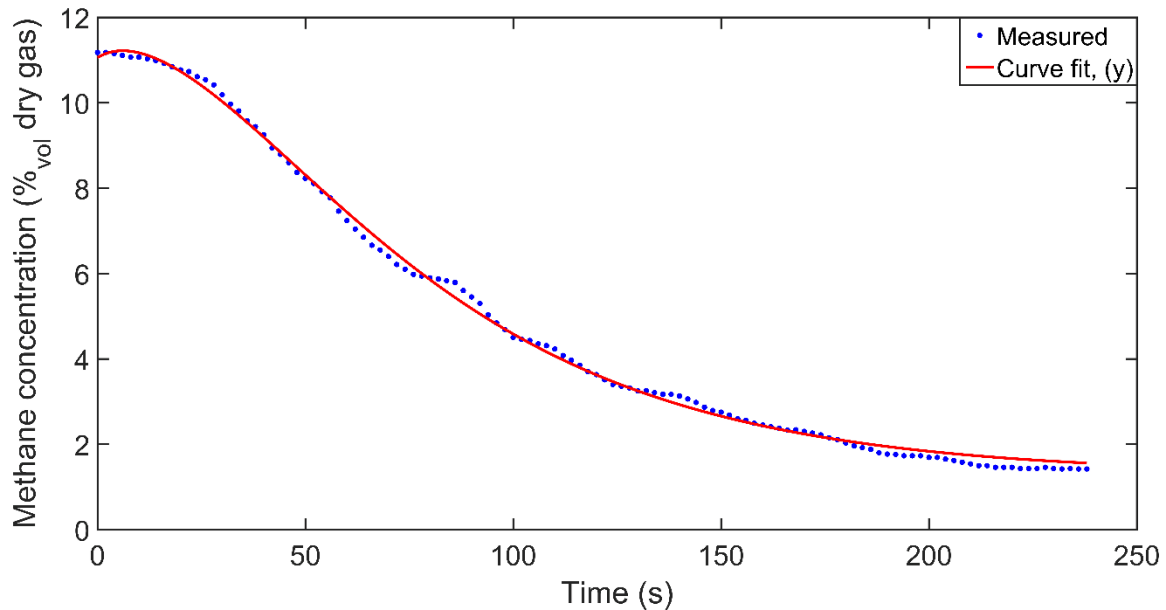


Figure 25: Measured concentration of methane over time following abrupt termination of fuel feeding. A function is fitted to the data, which are used in the subsequent deconvolution.

Despite the noise reduction obtained through curve fitting, the deconvolution is unstable, resulting in non-physical concentration values at around 10 s, where negative values occur, thereby explaining the gap in the graph in Figure 26. However, since the objective is to estimate the pyrolysis time, the absolute values of the estimated concentration of methane at the bed surface is not relevant. Instead, the time-point at which the concentration transient has decayed, indicating complete pyrolysis. From Figure 26, it is clear that the transient vanishes at around 70 s, which is roughly the time-point at which the fuel particles are observed with the camera in Paper VI. Thus, it seems likely that only those particles that are devolatilizing are captured by the camera.

Since the effect of the volatile matter that is being released from the particle is not reproduced in cold flow experiments, valuable information regarding solids mixing is gathered using a hot camera probe, even if it cannot capture particle motion after pyrolysis finishes. Thus, the combination of measurements from the high-temperature and cold flow experiments

complement each other. Thus, the complete fuel conversion process, *i.e.*, fuel mixing for both pyrolysing and non-pyrolysing particles, can be investigated.

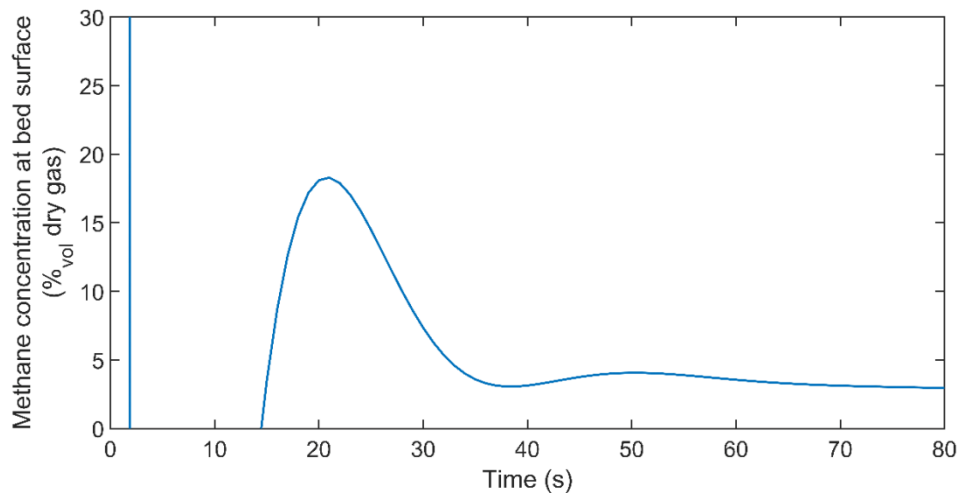


Figure 26: Estimated concentrations of methane at the bed surface using deconvolution. The transient vanishes at around 70 s, which is the estimated pyrolysis time.

7.4.1 Additional information obtained with the hot camera probe

The camera probe used in Paper VI has been upgraded over a period of several years so as to improve its robustness in relation to the harsh environment inside the Chalmers indirect gasifier. In the current version of the probe, a high-temperature-resistant lens is mounted at the front of the camera, which allows for the camera to be located further from the harsh environment at the probe tip and provides it with adequate cooling.

In an earlier version of the camera probe, the camera was placed at the probe tip without the additional temperature-resistant lens. With this configuration, the probe design allowed the use of a camera that was different from that used in Paper VI, providing a higher resolution and color video. With this system, unconverted char exiting the Chalmers CFB boiler could be observed at the bed surface of the indirect gasifier (Figure 27). At low fluidization velocities, the release of volatiles from the fuel fed to the gasifier could clearly be observed. The rapid release of volatiles increases the flotsam behavior of the fuel particles, an effect previously reported in the literature [14, 15, 34]. However, as the release of volatiles could not be captured visually at fluidization velocities >3-times the minimum fluidization velocity, the enhanced floatability is negligible at higher fluidization velocities.

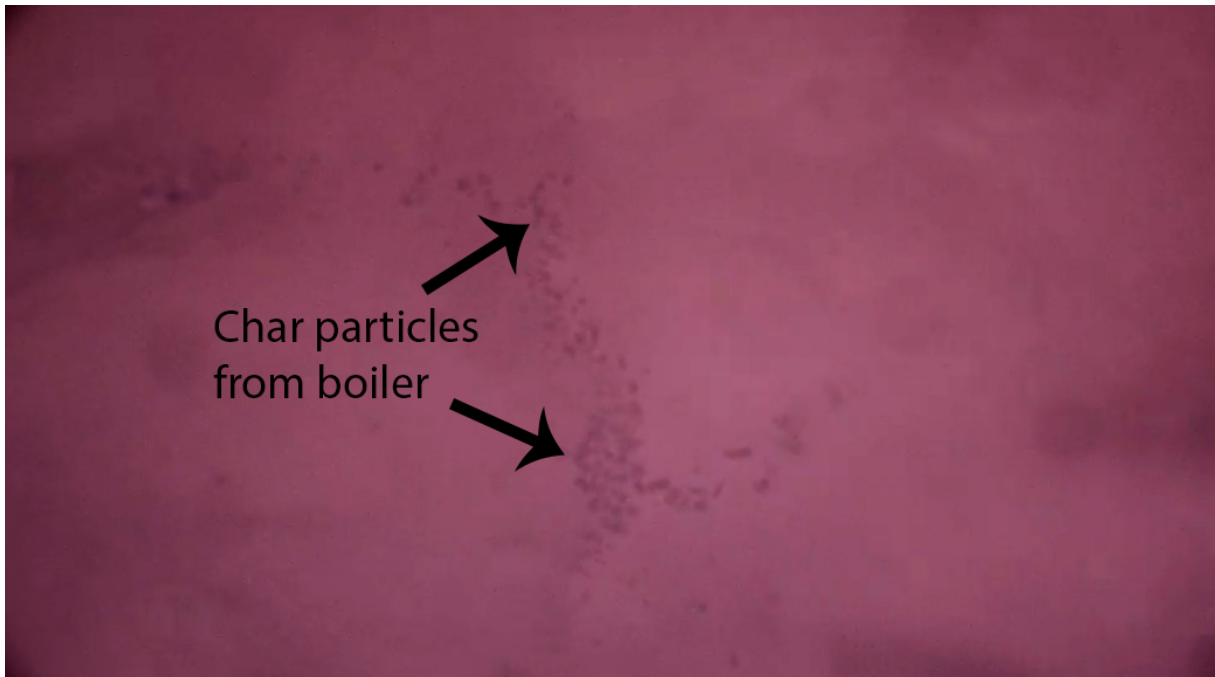


Figure 27: Char particles from the Chalmers boiler float on the bed surface of the Chalmers indirect gasifier while fluidized at $1.5U_{mf}$.

In summary, several particle-tracking techniques have been applied in this thesis. It is important to note that all of these techniques require the ability to distinguish individual particles, which limits the number of tracer particles that can be used. This in turn results in negligible interactions between the fuel particles, which is not what one would expect in industrial boilers and gasifiers (at least in proximity to the fuel-feeding locations). Thus, fluid-dynamic interactions between fuel particles need to be investigated by other means, either further developed experimental methods or through the use of mathematical modeling.

8 Conclusions

The conclusions of this work can be subdivided into: 1) those related to the bed material and fuel and the developed methods; and 2) those linked to the results of the experiments and the modeling.

8.1 Bed material

By applying fluid-dynamic downscaling, a lateral dispersion coefficient for bed material is obtained that is in the range of 10^{-3} – 10^{-2} , *i.e.*, up to two orders of magnitude higher than the values reported in the literature (sampled in lab-units without consideration to fluid-dynamic scaling). The lateral dispersion coefficient for the bed material increases with increases in the gas velocity and bed height, in line with increases in the bubble size. The lateral mixing of bed material is correlated with both bubble size and bubble frequency, which is in agreement with previous findings.

Lateral mixing of the bed material is induced by the bubble flow and has a dispersive nature, which can be well described by a diffusion equation. In the presence of a cross-flow of bulk solids, the macroscopic velocity field induced can be described by applying potential flow theory or using the Navier-Stokes equations for a single-phase flow.

8.2 Fuel

Three experimental methods to study the fuel mixing have been developed. First, a method was derived based on video recordings of the bed surfaces of fluid-dynamically downscaled units. Second, a cooled camera probe was designed and used to capture multiple individual fuel particles on the bed surface of the Chalmers gasifier operated at high temperature. Third, a magnetic particle tracking (MPT) method applicable to 3-dimensional, fluid-dynamically downscaled fluidized beds was developed. The spatial and temporal resolutions are approximately 1 mm and 1 ms, respectively. This provides sufficient accuracy to characterize the fuel flow patterns within the dense bed. Furthermore, a data processing algorithm has been developed and implemented that allows online tracking at 100 Hz. Taken together with the low cost of the components, the MPT technique is very competitive compared to the options previously used by fluidized bed investigators.

The applicability of fluid-dynamic downscaling to the mixing of fuel particles has been validated experimentally, thereby allowing cold flow models to be used in investigations of both bed materials and fuel particles. The lateral dispersive mixing of wood chips and pellets is strongly coupled to that of the bed material, while that of char shows a smaller dependence. In the presence of a solids cross-flow, there exists a slip between the induced convective mixing of the fuel and the convective field of the bulk solids. This slip decreases linearly with fluidization velocity, *i.e.*, the cross-flow impact factor increases with gas velocity. Tube bundles

fully decouple the lateral fuel mixing from the solids cross-flow. Furthermore, increased solids cross-flow reduces the vertical mixing of fuel.

The lateral mixing of fuel particles can be described by a convection-diffusion equation, which accounts for the dispersive mixing coupled to the bubble flow and the convective mixing related to the solids cross-flow.

9 Future work

During the course of this work, several avenues for future studies have emerged. These studies would improve the accuracy of the results and could also result in time savings in the experimental work.

9.1 Particle tracking in 3 dimensions

The MPT method has so far only been applied to bubbling fluidized beds. It is of obvious interest to apply it also to circulating fluidized beds. This should in theory be possible, although additional sensors will be required, some of which may need to be inserted into the bed to ensure that the magnetic tracer particle is never located too far from a sensor. Work to realize such a measurement system is ongoing. Furthermore, since the earth's magnetic field can influence the orientation estimation of the tracer, additional equipment is needed to counteract this background field.

As mentioned above, the tracer particle is currently not representative of low-density fuel particles and only cylindrical (*i.e.*, resembling pelletized fuel) geometries of the tracer particle have been used. In industrial-scale beds for biomass, it is more likely that wood chips are used as the fuel, which requires the use of tracer particles with other shapes and densities. Tests with such tracers are ongoing, although at the time of writing of this thesis, these measurements had not yet been evaluated.

9.2 Additional possibilities with camera measurements

The camera applied in the industrial-sized gasifier has to date only been used to evaluate the mixing of fuel particles. It should be possible to calibrate the camera against a source of known temperature, to investigate the temperature distribution over the bed surface. This system should be much less expensive to use than an IR camera.

Investigations of 2-dimensional fluidized beds have been performed to characterize the particle trajectory in the freeboard after a bubble eruption as being parabolic, whereby correlations for a ballistic object can be used to predict the motion. This behavior is likely to be similar in industrial-sized units, although this remains to be confirmed. Therefore, two cameras at slightly different positions could be calibrated for stereovision, which should resolve the 3D trajectories of the fuel particles in the freeboard.

9.3 Further investigations of cross-flow

Even though the influence of cross-flow has been investigated in this thesis, the experimental results should be confirmed and the modelling of the flow field should be developed further. Important features of both lateral and vertical mixing that are influenced by the cross-flow remain to be elucidated.

References

1. Koornneef, J., Junginger M., Faaij A., *Development of fluidized bed combustion-An overview of trends, performance and cost*. Progress in Energy and Combustion Science, 2007. **33**(1): p. 19-55.
2. Thunman, H., Seemann M.C. *First experiences with the new chalmers gasifier*. 2009.
3. Pfeifer, C., Puchner B., Hofbauer H., *Comparison of dual fluidized bed steam gasification of biomass with and without selective transport of CO₂*. Chemical Engineering Science, 2009. **64**(23): p. 5073-5083.
4. Hofbauer, H., Rauch R., Bosch K., Koch R., Aichernig C., *Biomass CHP plant Guessing-a success story*, in *Pyrolysis and Gasification of Biomass and Waste*, A.V. Bridgwater, Editor. 2003, CPL Press: Newbury, UK. p. 371-383.
5. Toshiyuki, S., Zhihong L., Makoto T., Koki H., Hidehisa T., *Gasification of Lignite Coal and Biomass Using Twin IHI Gasifier (TIGAR)*. IHI Engineering Review, 2012. **45**(1): p. 15-20.
6. Highley, J., Merrick D., *Effect of the spacing between solid feed points on the performance of a large fluidized bed reactor*. AIChE Symposium Series, 1971. **67**: p. 219-227.
7. Leckner, B., *Fluidized bed combustion: Mixing and pollutant limitation*. Progress in Energy and Combustion Science, 1998. **24**(1): p. 31-61.
8. Gómez-Barea, A., Leckner B., *Modeling of biomass gasification in fluidized bed*. Progress in Energy and Combustion Science, 2010. **36**(4): p. 444-509.
9. Knoebig, T., Luecke K., Werther J., *Mixing and reaction in the circulating fluidized bed - A three-dimensional combustor model*. Chemical Engineering Science, 1999. **54**(13-14): p. 2151-2160.
10. Ito, O., Kawabe R., Miyamoto T., Orita H., Mizumoto M., Miyadera M. *Direct Measurement of Particle Motion in a Large-Scale FBC Boiler Model*. in *The 15th International Conference on Fluidized Bed Combustion*. 1999. Savannah, USA: ASME.
11. Rowe, P.N., Nienow A.W., Agbim A.J., *The mechanism by which particles segregate in a gas fluidized bed*. Trans.I Chem.Engrs., 1972. **57**: p. 194-199.
12. Fotovat, F., Chaouki J., Bergthorson J., *Distribution of large biomass particles in a sand-biomass fluidized bed: Experiments and modeling*. AIChE Journal, 2014. **60**(3): p. 869-880.
13. Zhang, Y., Jin B., Zhong W., *Experimental investigation on mixing and segregation behavior of biomass particle in fluidized bed*. Chemical Engineering and Processing: Process Intensification, 2009. **48**(3): p. 745-754.
14. Solimene, R., Marzocchella A., Salatino P., *Hydrodynamic interaction between a coarse gas-emitting particle and a gas fluidized bed of finer solids*. Powder Technology, 2003. **133**(1-3): p. 79-90.
15. Bruni, G., Solimene R., Marzocchella A., Salatino P., Yates J.G., Lettieri P., Fiorentino M., *Self-segregation of high-volatile fuel particles during devolatilization in a fluidized bed reactor*. Powder Technology, 2002. **128**(1): p. 11-21.
16. Breault, R.W., *A review of gas-solid dispersion and mass transfer coefficient correlations in circulating fluidized beds*. Powder Technology, 2006. **163**(1-2): p. 9-17.
17. Abanades, J.C., Grasa G.S., *Modeling the Axial and Lateral Mixing of Solids in Fluidized Beds*. Industrial & Engineering Chemistry Research, 2001. **40**(23): p. 5656-5665.
18. Berruti, F., Scott D.S., Rhodes E., *Measuring and modelling lateral solid mixing in a three-dimensional batch gas-solid fluidized bed reactor*. Canadian Journal of Chemical Engineering, 1986. **64**(1): p. 48-56.
19. Borodulya, V.A., Epanov Y.G., Teplitskii Y.S., *Horizontal particle mixing in a free fluidized bed*. Journal of Engineering Physics, 1982. **42**(5): p. 528-533.
20. Fan, L.T., Song J.C., Yutani N., *Radial particle mixing in gas-solids fluidized beds*. Chemical Engineering Science, 1986. **41**(1): p. 117-122.

21. Kobayashi, N., Yamazaki R., Mori S., *A study on the behavior of bubbles and solids in bubbling fluidized beds*. Powder Technology, 2000. **113**(3): p. 327-344.
22. Lim, K.S., Agarwal P.K., *Circulatory motion of a large and lighter sphere in a bubbling fluidized bed of smaller and heavier particles*. Chemical Engineering Science, 1994. **49**(3): p. 421-424.
23. Lim, K.S., Gururajan V.S., Agarwal P.K., *Mixing of homogeneous solids in bubbling fluidized beds: Theoretical modelling and experimental investigation using digital image analysis*. Chemical Engineering Science, 1993. **48**(12): p. 2251-2265.
24. Mostoufi, N., Chaouki J., *Local solid mixing in gas–solid fluidized beds*. Powder Technology, 2001. **114**(1–3): p. 23-31.
25. Sette, E., Gómez García A., Pallares D., Johnsson F. *Quantitative evaluation of inert solids mixing in a bubbling fluidized bed*. in *21st International Conference on Fluidized Bed Combustion*. 2012. Naples, Italy.
26. Sette, E., Pallarès D., Johnsson F., *Experimental evaluation of lateral mixing of bulk solids in a fluid-dynamically down-scaled bubbling fluidized bed*. Powder Technology, 2014. **263**(0): p. 74-80.
27. Shi, Y.-F., Fan L.T., *Lateral mixing of solids in gas—solid fluidized beds with continuous flow of solids*. Powder Technology, 1985. **41**(1): p. 23-28.
28. Subbarao, D., Moghaddam E., Bannard J.E., *Lateral mixing of particles in fluidized beds*. Chemical Engineering Science, 1985. **40**(10): p. 1988-1990.
29. Valenzuela, J.A., Glicksman L.R., *An experimental study of solids mixing in a freely bubbling two-dimensional fluidized bed*. Powder Technology, 1984. **38**(1): p. 63-72.
30. Winaya, I.N.S., Shimizu T., Yamada D., *A new method to evaluate horizontal solid dispersion in a bubbling fluidized bed*. Powder Technology, 2007. **178**(3): p. 173-178.
31. Bellgardt, D., Werther J., *A novel method for the investigation of particle mixing in gas-solid systems*. Powder Technology, 1986. **48**(2): p. 173-180.
32. Berdugo Vilches, T., Sette E., Thunman H. *Behaviour of biomass particles in a large scale (2-4MWth) bubbling bed reactor*. in *Computational Methods in Multiphase Flow VIII*. 2015. Valencia, Spain: WIT Press.
33. Bi, J.C., Yang G.L., Kojima T., *Lateral mixing of coarse particles in fluidized beds of fine particles*. Trans IChem (Chemical Engineering Research and Design), 1995. **73**(A2): p. 162-167.
34. Chirone, R., Miccio F., Scala F., *On the relevance of axial and transversal fuel segregation during the FB combustion of a biomass*. Energy and Fuels, 2004. **18**(4): p. 1108-1117.
35. Liu, D., Chen X., *Lateral solids dispersion coefficient in large-scale fluidized beds*. Combustion and Flame, 2010. **157**(11): p. 2116-2124.
36. Nienow, A.W., Rowe P.N., Cheung L.Y.L., *A quantitative analysis of the mixing of two segregating powders of different density in a gas-fluidised bed*. Powder Technology, 1978. **20**(1): p. 89-97.
37. Niklasson, F., Thunman H., Johnsson F., Leckner B., *Estimation of solids mixing in a fluidized-bed combustor*. Industrial & Engineering Chemistry Research, 2002. **41**(18): p. 4663-4673.
38. Olsson, J., Larsson J., Sette E., Pallarès D., Sasic S., Johnsson F. *Experimental evaluation of the lateral mixing of fuel in a fluidized bed with cross-flow of solids - influence of tube banks*. in *11th International Conference on Fluidized Bed Technology, CFB 2014*. 2014. Beijing, China: Chemical Industry Press.
39. Olsson, J., Pallarès D., Johnsson F., *Lateral fuel dispersion in a large-scale bubbling fluidized bed*. Chemical Engineering Science, 2012. **74**: p. 148-159.
40. Pallarès, D., Díez P.A., Johnsson F. *Experimental analysis of fuel mixing patterns in a fluidized bed*. in *The 12th International Conference on Fluidization*. 2007. Vancouver, Canada: ECI.
41. Pallarès, D., Johnsson F., *A novel technique for particle tracking in cold 2-dimensional fluidized beds—simulating fuel dispersion*. Chemical Engineering Science, 2006. **61**(8): p. 2710-2720.

42. Rios, G.M., Dang Tran K., Masson H., *FREE OBJECT MOTION IN A GAS FLUIDIZED BED*. Chemical Engineering Communications, 1986. **47**(4-6): p. 247-272.
43. Schlichthaerle, P., Werther J., *Solids mixing in the bottom zone of a circulating fluidized bed*. Powder Technology, 2001. **120**(1-2): p. 21-33.
44. Sette, E., Aimé S., Pallares D., Johnsson F., *Analysis of lateral fuel mixing in a fluid-dynamically down-scaled bubbling fluidized bed*, in *Fluidization XIV Conference 2013*, ECI: Noordwijkerhout, The Netherlands. p. 877-884.
45. Sette, E., Pallarès D., Johnsson F., *Experimental quantification of lateral mixing of fuels in fluid-dynamically down-scaled bubbling fluidized beds*. Applied Energy, 2014. **136**(0): p. 671-681.
46. Sette, E., Pallarès D., Johnsson F., *Influence of bulk solids cross-flow on lateral mixing of fuel in dual fluidized beds*. Fuel Processing Technology, 2015. **140**: p. 245-251.
47. Sette, E., Pallarès D., Johnsson F., Ahrentorp F., Ericsson A., Johansson C., *Magnetic tracer-particle tracking in a fluid dynamically down-scaled bubbling fluidized bed*. Fuel Processing Technology, 2015. **138**(0): p. 368-377.
48. Soria-Verdugo, A., Garcia-Gutierrez L.M., García-Hernando N., Ruiz-Rivas U., *Buoyancy effects on objects moving in a bubbling fluidized bed*. Chemical Engineering Science, 2011. **66**(12): p. 2833-2841.
49. Soria-Verdugo, A., Garcia-Gutierrez L.M., Sanchez-Delgado S., Ruiz-Rivas U., *Circulation of an object immersed in a bubbling fluidized bed*. Chemical Engineering Science, 2011. **66**(1): p. 78-87.
50. Xiao, P., Yan G., Wang D., *Investigation on horizontal mixing of particles in dense bed in Circulating Fluidized Bed (CFB)*. Journal of Thermal Science, 1998. **7**(2): p. 78-84.
51. Sette, E., Berdugo Vilches T., Pallarès D., Johnsson F., *Measuring fuel mixing under industrial fluidized-bed conditions – A camera-probe based fuel tracking system*. Applied Energy, 2016. **163**: p. 304-312.
52. Glicksman, L.R., *Scaling relationships for fluidized beds*. Chemical Engineering Science, 1988. **43**(6): p. 1419-1421.
53. Johnsson, F., Vragar A., Leckner B. *Solids flow pattern in the exit region of a CFB-furnace-influence of exit geometry*. in *15th International Conference on Fluidized Bed Combustion*. 1999. Savannah, USA: ASME.
54. Stein, M., Ding Y.L., Seville J.P.K., *Experimental verification of the scaling relationships for bubbling gas-fluidised beds using the PEPT technique*. Chemical Engineering Science, 2002. **57**(17): p. 3649-3658.
55. Rowe, P.N., Partridge B.A., *An X-ray study of bubbles in fluidised beds*. Trans. Instn. Chem. Engrs., 1965. **43**: p. 157-175.
56. Werther, J., *Bubble chains in large diameter gas fluidized beds*. International Journal of Multiphase Flow, 1977. **3**(4): p. 367-381.
57. Andersson, S., Johnsson F., Leckner B. *Fluidization Regimes in non-slugging fluidized beds*. in *The 10th International Conference on Fluidized Bed Combustion*. 1989. San Francisco, USA: The American Society of Mechanical Engineers.
58. Baskakov, A.P., Tuponogov V.G., Filippovsky N.F., *A study of pressure fluctuations in a bubbling fluidized bed*. Powder Technology, 1986. **45**(2): p. 113-117.
59. Svensson, A., Johnsson F., Leckner B., *Bottom bed regimes in a circulating fluidized bed boiler*. International Journal of Multiphase Flow, 1996. **22**(6): p. 1187-1204.
60. Gustafsson, F., Ljung L., Millnert M., *Signal Processing*. 2010, Lund, Sweden: Studentlitteratur.
61. Hofbauer, H. *Scale up of fluidized bed gasifiers from laboratory scale to commercial plants: steam gasification of solid biomass in a dual fluidized bed system*. 2006.
62. Larsson, A., Seemann M., Neves D., Thunman H., *Evaluation of Performance of Industrial-Scale Dual Fluidized Bed Gasifiers Using the Chalmers 2–4-MWth Gasifier*. Energy & Fuels, 2013. **27**: p. 6665-6680.

63. Markström, P., Lyngfelt A., *Designing and operating a cold-flow model of a 100kW chemical-looping combustor*. Powder Technology, 2012. **222**: p. 182-192.
64. Thon, A., Kramp M., Hartge E.-U., Heinrich S., Werther J., *Operational experience with a system of coupled fluidized beds for chemical looping combustion of solid fuels using ilmenite as oxygen carrier*. Applied Energy, 2014. **118**: p. 309-317.
65. Bird, B., Stewart W., Lightfoot E., *Transport Phenomena*. 2 ed. 2007, New York, USA: John Wiley & Sons.
66. Kunii, D., Levenspiel O., *Fluidization Engineering*. 1991: Butterworth-Heinemann.
67. Coulson, J.M., Richardson J.F., Backhurst J.R., Harker J.H., *Chemical Engineering- Fluid Flow, Heat Transfer and Mass Transfer*. 6 ed. Vol. 1. 1999: Butterworth-Heinemann.
68. Buckingham, E., *On Physically Similar Systems; Illustrations of the Use of Dimensional Equations*. Physical Review, 1914. **4**(4): p. 345-376.
69. Glicksman, L.R., Hyre M.R., Farrell P.A., *Dynamic similarity in fluidization*. International Journal of Multiphase Flow, 1994. **20**(SUPPL. 1): p. 331-386.
70. Horio, M., Nonaka A., Sawa Y., Muchi I., *New similarity rule for fluidized bed scale-up*. AIChE Journal, 1986. **32**(9): p. 1466-1482.
71. Bonniol, F., Sierra C., Occelli R., Tadriss L., *Similarity in dense gas-solid fluidized bed, influence of the distributor and the air-plenum*. Powder Technology, 2009. **189**(1): p. 14-24.
72. Bricout, V., Louge M.Y., *A verification of Glicksman's reduced scaling under conditions analogous to pressurized circulating fluidization*. Chemical Engineering Science, 2004. **59**(13): p. 2633-2638.
73. Guío-Pérez, D.C., Pröll T., Hofbauer H., *Solids residence time distribution in the secondary reactor of a dual circulating fluidized bed system*. Chemical Engineering Science, 2013. **104**: p. 269-284.
74. Sanderson, J., Rhodes M., *Hydrodynamic similarity of solids motion and mixing in bubbling fluidized beds*. AIChE Journal, 2003. **49**(9): p. 2317-2327.
75. Leckner, B., Golriz M.R., Zhang, W., Andersson, B-A. *Boundary layers-First measurements in the 12 MW CFB research plant at Chalmers university*. in *11th International Conference on Fluidized Bed Combustion*. 1991. Montreal, Canada: ASME.
76. Chaouki, J., Larachi F., Duduković M.P., *Noninvasive Tomographic and Velocimetric Monitoring of Multiphase Flows*. Industrial and Engineering Chemistry Research, 1997. **36**(11): p. 4476-4503.
77. Banholzer, W.F., Spiro C.L., Kosky P.G., Maylotte D.H., *Direct imaging of time-averaged flow patterns in a fluidized reactor using x-ray computed tomography*. Industrial and Engineering Chemistry Research, 1987. **26**(4): p. 763-767.
78. Kantzas, A., *Computation of holdups in fluidized and trickle beds by computer-assisted tomography*. AIChE Journal, 1994. **40**(7): p. 1254-1261.
79. Simons, S.J.R., Seville J.P.K., Clift R., Gilboy W.B., Hosseini-Ashrafi M.E., *Application of gamma-ray tomography to gas fluidized and spouted beds*. Tomographic Techniques for Process Design and Operation, 1993: p. 227-238.
80. Kumar, S.B., Duduković M.P., *Chapter 2 - Computer assisted gamma and X-ray tomography: Applications to multiphase flow systems*, in *Non-Invasive Monitoring of Multiphase Flows*, J.C.L.P. Duduković, Editor. 1997, Elsevier Science B.V.: Amsterdam. p. 47-103.
81. Halow, J.S., Nicoletti P., *Observations of fluidized bed coalescence using capacitance imaging*. Powder Technology, 1992. **69**(3): p. 255-277.
82. Halow, J.S., Fasching G.E., Nicoletti P., Spenik J.L., *Observations of a fluidized bed using capacitance imaging*. Chemical Engineering Science, 1993. **48**(4): p. 643-659.
83. S., H.J., Fasching G.E., Nicoletti P., *Preliminary Capacitance Imaging Experiments of a Fluidized Bed*. AIChE Symposium Series, 1990. **86**(276): p. 41-50.

84. Thapa, R.K., Rautenbach C., Halvorsen B.M. *Investigation of flow behaviour in biomass gasifier using Electrical Capacitance Tomography (ECT) and pressure sensors*. in *11th International Conference on Polygeneration Strategies ICPS*. 2011. Vienna, Austria.
85. Yang, W., *Design of electrical capacitance tomography sensors*. Measurement science and technology, 2010. **21**.
86. Waterfall, R.C., He R., White N.B., Beck C.M., *Combustion imaging from electrical impedance measurements*. Measurement science and technology, 1996. **7**: p. 369-374.
87. Bemrose, C.R., Fowles P., Hawkesworth M.R., O'Dwyer M.A., *Application of positron emission tomography to particulate flow measurement in chemical engineering processes*. Nuclear Instruments and Methods in Physics Research Section A: Accelerators, Spectrometers, Detectors and Associated Equipment, 1988. **273**(2): p. 874-880.
88. Bemrose, C.R., Botteril J.S.M., Bridgwater J., Nienow A.W. *Large particle motion on the distributor of a fluidized bed of sand*. in *Fluidization V*. 1986.
89. Stein, M., Martin T.W., Seville J.P.K., McNeil P.A., Parker D.J., *Chapter 10 - Positron emission particle tracking: Particle velocities in gas fluidised beds, mixers and other applications*, in *Non-Invasive Monitoring of Multiphase Flows*, J.C.L.P. Duduković, Editor. 1997, Elsevier Science B.V.: Amsterdam. p. 309-333.
90. Kondukov, N.B., Kornilaev A.N., Skachko I.M., *An investigation of the parameters of moving particles in a fluidized bed by a radioisotopic method*. Int. Chem. Eng., 1964. **4**.
91. Van Velzen, D., Flamm H.J., Langenkamp H., Casile A., *Motion of solids in spouted beds*. The Canadian Journal of Chemical Engineering, 1974. **52**(2): p. 156-161.
92. Fotovat, F., Chaouki J. *The effect of biomass on the fluidization characteristics of biomass-sand mixtures*. in *The 21 st International Conference on Fluidized Bed Combustion*. 2012. Naples, Italy.
93. Godfroy, L., Larachi F., Kennedy G., Grandjean B., Chaouki J., *On-line flow visualization in multiphase reactors using neural networks*. Applied Radiation and Isotopes, 1997. **48**(2): p. 225-235.
94. Santana, D., Nauri S., Acosta A., García N., Macías-Machín A., *Initial particle velocity spatial distribution from 2-D erupting bubbles in fluidized beds*. Powder Technology, 2005. **150**(1): p. 1-8.
95. Buist, K.A., van der Gaag A.C., Deen N.G., Kuipers J.A.M., *Improved magnetic particle tracking technique in dense gas fluidized beds*. AIChE Journal, 2014. **60**(9): p. 3133-3142.
96. Idakiev, V., Mörl L., *How to measure the particle translation and rotation in a spouted and fluidized bed?* Journal of Chemical Technology and Metallurgy, 2013. **48**(5): p. 445-450.
97. Mohs, G., Gryczka O., Heinrich S., Mörl L., *Magnetic monitoring of a single particle in a prismatic spouted bed*. Chemical Engineering Science, 2009. **64**(23): p. 4811-4825.
98. Neuwirth, J., Antonyuk S., Heinrich S., Jacob M., *CFD-DEM study and direct measurement of the granular flow in a rotor granulator*. Chemical Engineering Science, 2013. **86**: p. 151-163.
99. Danckwerts, P.V., *Continuous flow systems. Distribution of residence times*. Chemical Engineering Science, 1953. **2**: p. 1-13.
100. Fogler, S.H., *Elements of Chemical Reaction Engineering*. Vol. 4. 2004: Prentice Hall.
101. Harris, A.T., Davidson J.F., Thorpe R.B., *A novel method for measuring the residence time distribution in short time scale particulate systems*. Chemical Engineering Journal, 2002. **89**(1-3): p. 127-142.
102. Kalman, R.E., *A New Approach to Linear Filtering and Prediction Problems*. Transactions of the ASME-Journal of Basic Engineering, 1960. **82**: p. 35-45.
103. Simon, D., *Optimal State Estimation-Kalman, H_∞, and Nonlinear approaches*. 2006, Hoboken, New Jersey, USA: John Wiley & Sons.
104. Eriksson, L., Johansson E., Kettaneh-Wold N., Wold S., *Multi- and Megavariate Data Analysis-Principles and Applications*. 2006, Umeå, Sweden: Umetrics Academy.

105. Shi, Y.-f., Fan L.T., *Lateral mixing of solids in batch gas-solids fluidized beds*. Industrial & Engineering Chemistry, Process Design and Development, 1984. **23**(2): p. 337-341.
106. Larsson, A., *FUEL CONVERSION IN A DUAL FLUIDIZED BED GASIFIER*
- EXPERIMENTAL QUANTIFICATION AND IMPACT ON PERFORMANCE*, in *Dept. of Energy and Environment*. 2014, Chalmers University of Technology: Göteborg.
107. Iqbal, M., *Deconvolution and regularization for numerical solutions of incorrectly posed problems*. Journal of Computational and Applied Mathematics, 2003. **151**(2): p. 463-476.